CHAPTER VI

DIAGENESIS

This chapter is intended to depict the diagenetic textures that have been recorded in the rocks of the Khao Khad Formation. The processes to produce those textures will also be explored and interpreted in terms of depositional environment. Finally such information will lead to the reconstruction of diagenetic evolution of post Permian rocks in the central Thailand.

This chapter will be divided into 1) general statement of diagenesis, 2) elemental compositions in carbonate constituents, 3) cathodoluminescence, 4) stable oxygen and carbon isotopes, 5) carbonate constituents, 6) diagenetic processes, and 7) diagenetic evolution. In each diagenetic process there will be a petrographic texture, their association and interpretation. Bulk elemental and stable isotopic compositions are present in separate section earlier mentioned.

6.1 General Statement of Diagenesis

The diagenesis of carbonate sediments involve all processes acting upon these materials after their initial deposition. Such processes include alteration, dissolution, cementation and lithification between deposition and subsequent metamorphism. It is generally recognized as physical, chemical and organic processes acting upon carbonate sediments since deposition. They have a strong influence on changing mineralogy, sedimentary textures and structures. In many cases, the diagenetic textures related to lithification can be confused with primary depositional structures and textures. Therefore knowing the diagenetic processes is extremely important for

distinguishing the original depositional textures or structures from those of diagenesis, and also help in the interpretation of depositional environment.

The diagenesis of carbonate rocks can be deciphered from the study of both modern and ancient carbonate sediments. In modern carbonate sediments the original mineralogy, and sedimentary textures and structures are generally well preserved. In ancient carbonates, the rocks are usually dominated by subsequent diagenetic fabrics.

6.2 Elemental Compositions of Carbonate Constituents

In this study, nine elements including Ca, Mg, Fe, Mn, Na, Sr, Ba, K, and Si were analyzed on various carbonate and non-carbonate components. The detailed results of the analyses are shown in Appendix A. The Ca and Mg are considered as the major element in calcite and dolomite, respectively, and the Si is major element in quartz. In general, the overall values of minor and trace elements (Mg, Fe, Mn, Na, Sr, Ba and K) of various carbonate components of the rocks of the Khao Khad Formation are relatively low and inconsistent. The concentrations of Mg and Sr in most calcite component are usually lower than the detection limits of the EPMA ($<$ 6 ppms for Mg and $<$ 295 ppms for Sr), except in part of dolomite where the Mg can be detected. It is noted that the low content of trace elements in the Khao Khad Formation is similar to those found in the Ratburi limestone (Baird, 1992) and Nam Maholan Formation in Loei (Assavapatchara, 1998).

The Khao Khad Formation contains low Sr concentration (below the detection limit of EPMA of 295 ppms) similar to those found in Ratburi limestone. Braid (1992) found low concentration of Sr in both calcite and dolomite in the Permian Ratburi limestone and suggested that they were compatible with ancient marine value. The

concentration of Sr in ancient carbonate rocks usually low due to its loss during diagenesis.

Carbonate minerals in sediments are commonly occurs as $CaCO_3$ in the form of aragonite and calcite which ideally contains only Ca^{2+} as cation in crystal lattices. Some other cations having ionic radii approaching that of Ca^{2+} could also form as carbonate minerals in the same crystal system as aragonite or calcite. For examples Cd could form as otavite, Mn as rhodochrosite, Fe as siderite, Zn as smithsonite. For this reason, many cations of similar charge and ionic radii can substitute for Ca^{2+} as minor or trace elements in aragonite and calcite. The divalent cations with ionic radii smaller than that of Ca^{2+} (1.00 Å), such as Mg^{2+} (0.72 Å), Fe^{2+} (0.78 Å) and Mn^{2+} (0.83 Å) tend to substitute for calcium in calcite lattice. On the other hand, some cations with ionic radii larger than that of calcium, such as Sr^{2+} (1.31 Å), Pb^{2+} (1.35 Å) and Ba^{2+} (1.47 Å) are incorporated in the aragonite lattice (Dickson, 1990; Morse and Mackenzie, 1990).

The incorporation of a trace element into the carbonate lattice is governed by the distribution coefficient (D) and the element concentration in the precipitating fluid as the equation followed:

$$D = (^{m}Tr_s/^{m}Ca_s)_f / (^{m}Tr_l/^{m}Ca_l)_f \qquad \text{(Dickson, 1990)}$$

Where D is the homogeneous distribution coefficient; m is the molar concentration; Tr is the guest or trace constituent; Ca is the host constituent or Ca^{2+} in the case of calcite; s is solid and l is liquid; and f is the final concentration.

The distribution coefficient of Mg, Mn, Fe, Na and Sr for aragonite, calcite and dolomite (referred to Dickson, 1990; Vahrenkamp and Swart, 1990; and Veiser, 1983) are tabulated in Table 6.1.

Table 6.1 The distribution coefficient of trace element in aragonite, calcite and dolomite (Dickson, 1990; Vahrenkamp and Swart, 1990; and Veiser, 1983)

Minor and trace elements	Distribution coefficient (D)			References
	Aragonite	Calcite	Dolomite	
Mg	-	0.01-0.03	-	Dickson (1990)
Mn	-	10	-	Dickson (1990)
Mn	0.86	5.4-30	-	Veiser (1983)
Fe	-	5	-	Dickson (1990)
Fe	-	1<X<20	-	Veiser (1983)
Na	0.00014	0.00003	-	Veiser (1983)
Sr	0.9-1.2	0.027-0.04	0.025-0.06	Veiser (1983)
Sr	-	-	0.0118	Vahrenkamp and Swart (1990)

The distribution coefficients show that calcite favors the incorporation of Fe and Mn and aragonite favors the incorporation of Sr and Na. In a close system, the precipitation of crystal from a solution can affect the trace to host ratio of the liquid, the so-called 'heterogeneous precipitation'. The concentration of the component in the liquid relative to the host changes as precipitation proceeds. So the concentration of that constituent in the calcite will vary. If no adjustment has taken place in the solid, the elementally zoned crystal would occur (Dickson, 1990). In the open system, precipitation will be occurred in equilibrium due to continuous supply of trace element through the liquid flow and unique trace element concentration in calcite will be occurred.

The normal seawater contains relatively high contents of Na, Mg, Ca and Sr with the means of 10,800, 1,290, 411 and 8.1 ppms and low contents of Ba, Fe and Mn with the means of 0.021, 0.0034 and 0.0004 ppm, respectively (Turekian, 1968). Theoretically, using the coefficient data mentioned earlier, the minor and trace element

content of precipitated seawater carbonate can be determined from the element concentration of normal seawater. The contents of Sr, Na and Mn in aragonite precipitated from seawater are about 7094.92 to 9459.89, 1471.53 and 0.335 ppms, respectively. The contents of Mg, Na, Sr and Mn in calcite precipitated from seawater are about 12554.75 to 37664.24, 3.31 to 678.89, 212.85 to 315.33 and 2.1 to 11.68 ppms, respectively. The content of Sr in dolomite is about 93 to 473 ppms.

As the carbonate sediments undergo diagenetic alteration, the diagenetic fluid that were in contact with those burial sediments should have elemental composition ranging between those of marine and meteoric water. The latter is increasingly more common and well constrained fluid in late diagenesis. The concentration of dissolved iron and manganese in both marine and meteoric waters are usually low reflecting an oxic nature of these fluids. Here, both ions are in oxidized forms, such as Fe^{3+}, Mn^{3+} and Mn^{4+} which are not suitable in calcite crystal lattices. Hence the carbonate cements precipitated from marine or meteoric water during diagenesis in oxic condition would favor the formation of low Fe and Mn calcite. However, some carbonate cements containing high contents of Fe and Mn are usually originated from meteoric water in anoxic (negative Eh) condition.

6.3 Cathodoluminescence

Cathodoluminescence (CL) has become an important tool for distinguish diagenetic events. Cement stratigraphy can be differentiated by the difference in luminescence. It is a powerful tool to distinguish chemical and crystallographic zonation, define paragenetic sequences, evaluate crystal growth histories, and assess recrystallization of grains and cements. It can also be used in studying of diagenetic patterns in carbonate strata (e.g. Dorobek, 1987; Goldstein, 1988; Grover and Read, 1983; Kaufman et al., 1988; Major et al., 1988; Meyers 1978; Meyers and Lohmann

1985; Niemann and Read, 1988; O'Neill, Manger and Hays, 2003; and Solomon and Walkden, 1985).

Calcite typically shows a bright luminescence if it contains Mn^{2+} in the amount of a few hundred to a few thousand ppms and the Fe^{2+} ion can serve as a quencher (Marshall, 1988). Bud et al. (2000) reported that about 25 ppms Mn was necessary to initiate CL and the CL intensity is strictly a function of Mn content. Not until concentration of Fe reaches 100 ppms, then it is sufficient to exert a quenching effect. The advance of high resolution analytical techniques such as the electron microprobe and ion microprobe has allowed quantitative measurement of activator, sensitizer and quencher elements in relation to the luminescence in calcite and dolomite (e.g. Bud et al., 2000; Fairchild, 1983; Frank et al., 1982, Grover and Read, 1982; Habermann et al., 1996, 1998; Hemming et al., 1989; Major and Wilber, 1991; Meyers and Lohmann, 1985; Pierson, 1981; Savard et al., 1995). Hemming et al. (1989) concluded that CL intensities positively correlate with Mn concentrations at approximately constant Fe/Mn ratio within narrow ranges of Fe contents. Low Fe content (<1,000 ppms) will cause the CL intensity more sensitive to Mn activator than to Fe quencher. The Fe contents up to 10,000 ppms still do not extinguish Mn activated CL in calcite. The Mn contents more than 100 ppms will luminesce even in the presence of moderate amounts of Fe. In the absence of detectable Fe, calcite containing about 150 – 650 ppms Mn will show moderate CL and with the Mn content greater than 700 ppms, it will show bright CL.

The luminescence color of calcite in cathodoluminoscope is usually a combination of yellow, orange and red. Dolomite commonly shows more red color toward the red end of the spectrum than that of calcite. However, these colors are only a guide due to the variation in diagenetic environment. The dark and bright zones of luminescence are caused by variation of ion in fluid which could occur by fluctuating

Eh. The increasing of Mn contents in precipitating calcite can be due to increasing supersaturation of the fluid (Ten Have and Heijnen, 1985). With increasing burial depth, water will become anoxic and so the Mn contents will increase, this will give orange luminescence in calcite. In the deeper burial regime, out of the meteoric phreatic zone, Fe content will increase and so act as a quencher, producing dull luminescence in calcite (Grover and Read, 1983).

So, the variation of luminescence in sedimentary sequence of the Khao Khad Formation may indicate that the non-luminescence occurs in the oxic meteoric and marine realms, the bright luminescence occurs in anoxic burial diagenesis, and dull luminescence may occur in the deep burial. The multiple parallel zoning may indicate the variation in elemental composition which favors pore fluid in a close system. The author will use the trace element data as supporting evidences to explain the features revealed by cathodoluminescence and staining in later sections.

6.4 Oxygen and Carbon Isotopes

The carbon and oxygen isotopic signature of limestone has widely been accepted in diagenetic study. Many previous authors have examined the behavior of carbon and oxygen isotopes in carbonate sediments and their diagenesis such as Anderson and Arthur (1983), and Dickson (1990).

Bicarbonate ion in seawater is a major source of carbon in precipitating carbonate minerals in marine environment. However, the stable oxygen and carbon isotope compositions of marine carbonates depend on temperature and salinity of sea water (Hudson, 1977), their mineralogy, and biochemical fractionation (Wagener, 1975; Rao, 1990). Fractionation of oxygen isotopes of water at the earth's surface occurs by evaporation and condensation which depends on temperature, latitude and

altitude. The preferential evaporation of ^{16}O from seawater produces depleted in $^{18}O/^{16}O$ of meteoric water and increase in $^{18}O/^{16}O$ of seawater, but due to the large ocean reservoir, marine values show much smaller variations in $^{18}O/^{16}O$ (Anderson and Arthur, 1983). Moreover, meteoric waters may contain lighter carbon isotope caused by atmospheric and organic carbon derived in soils (Anderson and Arthur, 1983). The carbonate skeletons produced by living organism contain different isotopic composition from dissolved bicarbonate and inorganic precipitation due to fractionation during respiration or photosynthesis of living organisms. The fractionation of $^{13}C/^{12}C$ due to increasing temperature seems to be insignificant (Dickson, 1990), although Emrich et al. (1970) gave a temperature dependent fractionation during precipitation of calcium carbonate of about 0.035 ‰ per $^\circ$C. The fractionation of 18O/16O in the calcium carbonate-water-bicarbonate system has been suggested for paleotemperature reconstruction of ancient ocean since 1947 (Dickson, 1990). The fractionation was established by Epstein et al. (1953) and modified by Craig (1965) as:

$$T\,(^\circ C) = 16.9 - 4.2\,(\delta c - \delta w) + 0.13(\delta c - \delta w)^2 \qquad \text{(Dickson, 1990)}$$

Where T is temperature; δc is the $\delta^{18}O$ of CO_2 produce by reaction of $CaCO_3$ in phosphoric acid at 25 $^\circ$C; and δw is the $\delta^{18}O$ of CO_2 in equilibrium with water at 25 $^\circ$C, both PDB.

The original isotopic composition of carbonate minerals were subsequently altered as they were affected by meteoric water or undergo burial diagenesis. These changes depend on the variation of the $\delta^{18}O/^{16}O$ and $\delta^{13}C/^{12}C$ values of formation solution which depend on latitude, altitude, salinity of precipitating solution, seasonal of meteoric water, temperature and degree of diagenesis (Allan and Mathews, 1977; Brand and Veizer, 1980; Rao, 1989). Thus, the study of variation of isotopic

composition in carbonate minerals is useful in diagenetic interpretation. This study therefore will deal with the isotopic composition of individual carbonate components, and compare to those of Permian seawater carbonates and the Permian carbonates from other localities.

6.4.1 Original Isotopic Composition of Permian Seawater Carbonates

The original stable isotope compositions of Permian seawater carbonates were actually not known, but many researchers proposed the values from the least altered fabrics. Theoretically, the samples should be free of any diagenetic and metamorphic overprint (Veizer, 1983). Essentially, the Fe and Mn content in shallow seawater are low and they are not favor to incorporate into aragonite due to the low distribution coefficient of both elements in aragonite. Thus, the stable isotopic values of Permian aragonite should reflect the original stable isotope compositions of Permian seawater. But in fact there is rarely any Permian aragonite being left in carbonate rocks. Nonetheless, Given and Lohmann (1985) gave the isotopic compositions of non-luminescent aragonite and calcite in Permian marine cement from the El Capitan Reef, having the $\delta^{18}O$ values from -0.7 to -2.8 ‰PDB and the $\delta^{13}C$ values from 5.2 to 5.8 ‰PDB.

6.4.2 The Isotopic Composition of Various Diagenetic Fabrics

In this study the author separated carbonate samples from different diagenetic fabrics using a dental drill for the stable oxygen and carbon isotope analyses. They include calcareous allochems, micrite matrix, various calcite cements and associated calcite veins. However, as for the fine calcarenite and calcilutite which consists of very fine materials, they were analyzed as whole rock samples. The results are summarized in the following sections and details are given in Appendix B.

6.4.2.1 Calcareous Allochems

Calcareous allochems separated for the isotopic analysis are brachiopod shell, crinoid fragments, intraclasts and micritized fusulinid shells. The brachiopod shell (a well preserved and non-luminescing calcite most probably representing original carbonate component) has $\delta^{18}O$ value of -4.78 ‰PDB and $\delta^{13}C$ value of -0.67 ‰PDB. The crinoid fragments (14 samples) have the $\delta^{18}O$ values from -6.91 to -2.31 ‰PDB and the $\delta^{13}C$ value from 3.25 to 5.02 ‰PDB. The intraclasts (3 samples) have the $\delta^{18}O$ values from -9.58 to -6.06 ‰PDB and the $\delta^{13}C$ values from 3.68 to 4.27 ‰PDB. The micritized fusulinid shells (3 samples) have the $\delta^{18}O$ values from -8.93 to -6.18 ‰PDB and the $\delta^{13}C$ values from 0.11 to 4.24 ‰PDB.

6.4.2.2 Micrite Matrix

Different types of micrite matrix were recognized based on color as greenish grey, black, brownish grey and dark grey micrites. The greenish grey micrite has the $\delta^{18}O$ and $\delta^{13}C$ values of -7.83 ‰PDB and 3.66 ‰PDB, respectively. The black micrites (7 samples) have the $\delta^{18}O$ values from -10.85 to -4.95 ‰PDB and the $\delta^{13}C$ values from 0.58 to 5.49 ‰PDB. The brownish grey micrite has the $\delta^{18}O$ and $\delta^{13}C$ values of -7.74 ‰PDB and -0.3 ‰PDB, respectively. The dark grey micrites (11 samples) have the $\delta^{18}O$ values from -9.73 to -2.83 ‰PDB and the $\delta^{13}C$ values from 0.54 to 4.81 ‰PDB.

6.4.2.3 Calcite Cements

Several types of calcite cements analyzed for isotope composition are fibrous, syntaxial overgrowths and equant calcite cements. The fibrous calcite cements (2 samples) have the $\delta^{18}O$ values from -6.13 and -4.44 ‰PDB and the $\delta^{13}C$ value from

1.69 and 2.88 ‰PDB. The syntaxial overgrowths calcite cements (3 samples) have the $\delta^{18}O$ values from –6.83 to -4.37 ‰PDB and the $\delta^{13}C$ values from 2.91 to 3.58 ‰PDB. The equant calcite cements (10 samples) have the $\delta^{18}O$ values from -7.25 to -4.78 ‰PDB and the $\delta^{13}C$ values from 0.92 to 4.82 ‰PDB.

6.4.2.4 Calcite Veins

Two types of calcite veins, namely non-ferroan and ferroan sparry calcite, were analyzed for isotopic composition. The non-ferroan calcites (3 samples) have the $\delta^{18}O$ values from -9.45 to -5.77 ‰PDB and the $\delta^{13}C$ values from 4.01 to 4.83 ‰PDB. The ferroan calcites (4 samples) have the $\delta^{18}O$ values from -16.75 to -11.68 ‰PDB and the $\delta^{13}C$ values from 1.87 to 4.09 ‰PDB.

6.4.2.5 Whole Rock Samples

Whole rock samples recognized as dolomitic and non-dolomitic limestones were also analyzed for the isotopic composition. The whole-rock dolomitic limestones (2 samples) have the $\delta^{18}O$ values of -7.60 and -5.42 ‰PDB and the $\delta^{13}C$ values of -4.65 and 4.77 ‰PDB. The whole-rock non-dolomitic limestones (20 samples) have the $\delta^{18}O$ values from –7.03 to –3.74 ‰PDB and the $\delta^{13}C$ values from -1.05 to 4.91 ‰PDB.

All the isotopic values of individual carbonate components and the whole-rock samples are plotted in Figure 6.1. Also included in this diagram are the isotopic values of the original Permian seawater carbonates reported by Given and Lohman (1985). It appears that the isotopic signature of the individual diagenetic fabrics and the whole-rock carbonate samples are somewhat lighter in both $\delta^{18}O$ and $\delta^{13}C$ than those of the original Permian marine cement reported by Given and Lohmann (1985).
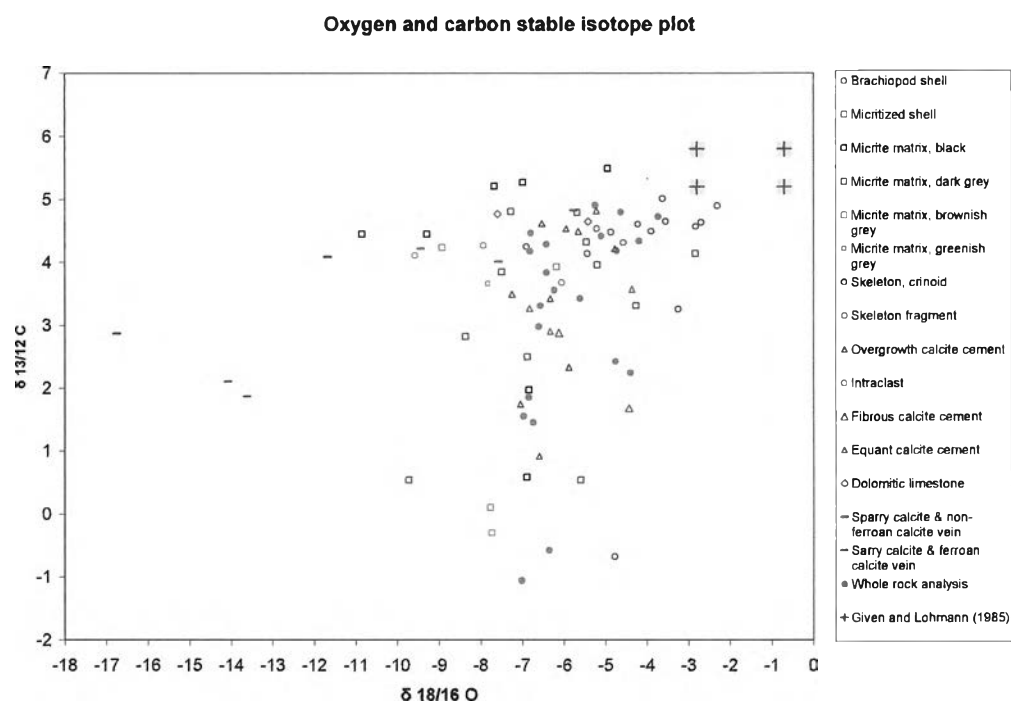
Oxygen and carbon stable isotope plot

Figure 6.1 The δ^{18}O and δ^{13}C cross- plot of various carbonate fabrics of the Khao Khad

Formation and original Permian seawater carbonates.

They, however, show a spread out from the $\delta^{18}O$ and $\delta^{13}C$ values of Given and Lohmann (1985). In fact, a well preserved and non-luminescing calcite drilled from the brachiopod shell, which is most probable represent original carbonate component, still has the isotopic compositions (-4.78 ‰ for $\delta^{18}O$ and -0.67‰ $\delta^{13}C$) somewhat lighter. Even though the overall isotopic signature of these carbonates, especially the carbon isotopes (mostly heavier than 0‰), still reflect the marine source, they were probable subjected to certain degree of isotopic exchange with lighter isotopic sources, such as organic carbon or freshwater carbonate in meteoric water during burial diagenesis. This can be seen from the $\delta^{18}O$ values of the late ferroan (suggesting meteoric origin) vein calcite that are clearly differentiate from those of the carbonates.

6.4.3 Comparison with Other Permian Carbonates

The isotopic values of carbonates are compared between the Khao Khad Formation, the Ratburi limestone (data from Baird, 1992) and Nam Maholan Formation (data from Assavapatchara, 1998) in Figure 6.2. The isotopic signature of the Khao Khad Formation and the Nam Maholan Formation are grouped in the same values but the Ratburi limestone shows much wider variation in a number of samples. This suggests that the Khao Khad Formation and the Nam Maholan Formation might have nearly the same isotopic modification whereas the Ratburi stronger degree of isotopic modification during diagenetic evolution.

6.5 Carbonate Constituents

In this section the carbonate constituents of the Khao Khad Formation will be summarized in terms of texture, trace element composition and environment of deposition. As a matter of fact, the carbonate constituents of the Khao Khad Formation consist of both allochems and orthochems (Folk, 1959). The allochemical constituent

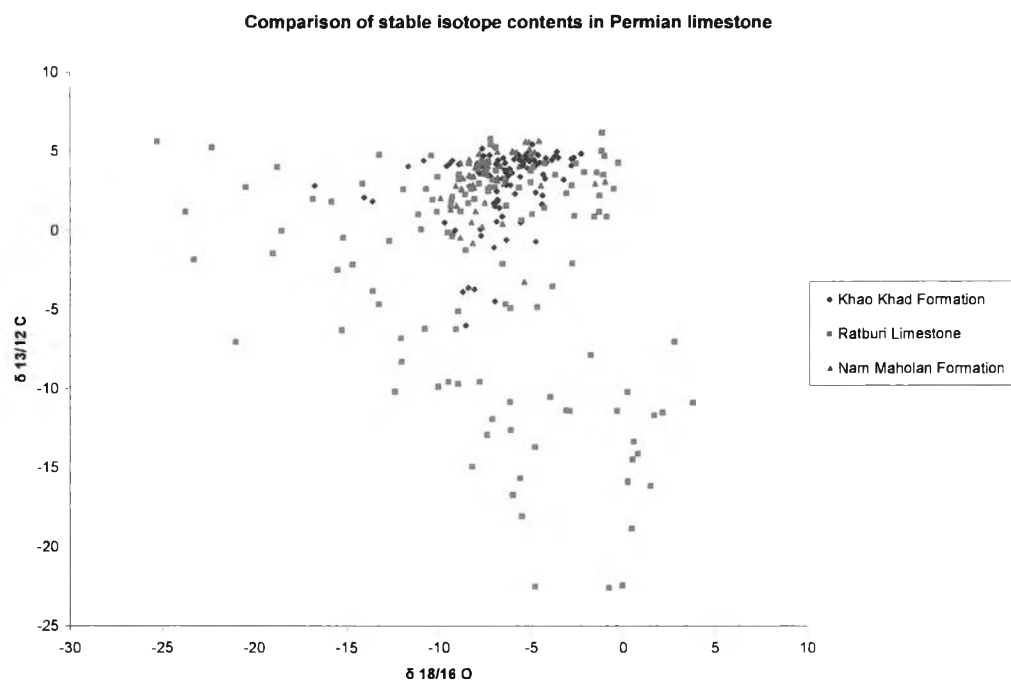Comparison of stable isotope contents in Permian limestone

Figure 6.2 The $\delta^{18}O$ and $\delta^{13}C$ cross plot of the Khao Khad Formation, Ratburi limestone and Nam Maholan Formation.

consists of four types, namely, fossils or bioclasts, intraclasts, pellets and oncoid. The bioclasts are fusulinid tests, crinoid fragments, brachiopod shells, gastropod shells, bryozoa and algal fragments. The orthochemical constituents consist of micrite and sparry calcite cement. They were affected by various degrees of alterations including mechanical, biological and chemical processes.

6.5.1 Fusulinid Tests

Fusulinid tests are a dominant bioclast in the Khao Khad area and the Pak Chong to Khao Yai area and common in the Khao Chan area. They are mainly found as nearly complete shells with some are broken fragments. The sizes of fusulinid test vary from 1 to 12 mms. Shell surface are usually coated by a thin-layer of dark micrite. Internal structures, i.e., spirotheca and keriotheca, were usually obscured due to the micritization or replaced by sparry calcite. The trace element composition of fusulinid tests are given in micritization section (6.6.1.1).

6.5.2 Crinoid Fragments

Crinoid fragments are another major grain component in the Khao Chan area and also common in the Khao Khad area. The fragments vary from 0.5 mm to 2 cms in size. The original crinoid ossicles, which presently appear as a single crystal, was commonly abraded into a rounded grain. The grain was also micritized and overgrowths by calcite cement. The cementation was usually developed in optical continuity to the host grain, call syntaxial overgrowths (Bathurst, 1958).

The trace element compositions of crinoid fragments (16 samples) are summarized in Table 6.2 and details are shown in Appendix A. They contain moderate

concentration of Na, Mn, Fe, K, Si and K, respectively in degree of abundance. The Mg and Sr contents are below the detection limit of EPMA.

Table 6.2 Summary of trace element contents of crinoid fragments

	Elemental composition of crinoid fragments (ppm)									
	Ca	Mg	Fe	Mn	Na	Sr	Ba	K	Si	Total
Min	387,120.77	0.00	0.00	100.68	0.00	0.00	0.00	0.00	0.00	387,621.43
Max	418,724.51	0.00	963.87	937.09	919.90	0.00	206.00	614.31	1,037.77	419,673.04
Average	403,439.45	0.00	193.36	263.32	342.18	0.00	43.66	134.90	122.13	404,538.99
SD	9,180.75	0.00	262.33	209.78	279.08	0.00	61.70	155.97	264.67	9,065.03

6.5.3 Brachiopod and Gastropod Shells

Brachiopod and gastropod shells are also a common grain component in the Khao Khad area and the Pak Chong to Khao Yai area. Shells are found as small and large fragments of few mms to several cms in size. The internal structures usually obscured by coarsely crystalline calcite. However, some of brachiopod and gastropod shells are well preserved locally in the Pak Chong to Khao Yai area.

The trace element composition of well preserved brachiopod shells (15 samples) are summarized in Table 6.3 and details in Appendix A. They show rather low concentration of Na, Ba, Fe, Mn, Sr and K. The Mg and Si content are below the detection limit of EPMA.

6.5.4 Bryozoa Fragments

Bryozoa fragments are common in the three studied areas and usually associated with crinoid fragments. They appear as micritized fragments less than one mm in size.

Table 6.3 Summary of trace element concentrations of well preserved brachiopod shells.

	Elemental composition of brachiopod shells (ppm)									
	Ca	Mg	Fe	Mn	Na	Sr	Ba	K	Si	Total
Min	380,309.74	0.00	0.00	0.00	0.00	0.00	0.00	0.00	0.00	380,745.10
Max	400,749.97	0.00	225.42	139.40	489.62	295.96	268.70	99.62	0.00	401,239.59
Average	390,852.90	0.00	55.97	43.89	126.61	19.73	84.79	11.07	0.00	391,194.95
SD	5,461.83	0.00	71.19	48.34	159.98	76.42	102.84	29.88	0.00	5,444.56

6.5.5 Algal Fragments

Algal fragments are dominant in the Khao Khad and Pak Chong to Khao Yai areas, and also common in the Khao Chan area. They are found as small fragments associated with biomicrite. The algal coated stromatolites are abundant in the lower part of the Khao Khad area. The occurrence of algal stromatolite is generally indicated shallow hardground area in relatively high-energy environments (Monty, 1965 and Peryt, 1975 cited in Flügel, 1982).

6.5.6 Intraclasts

Intraclasts (Folk, 1959) are dominant in the Khao Chan area and minor in the Khao Khad and the Pak Chong to Khao Yai areas. They are found as irregular shape of aggregate grains. The abraded margin cuts indiscriminately across former grains of host semi-consolidated sediment. Intraclasts occur in different shapes and size (<1 mm to several cms). Their internal fabric mainly consists of micrite. The occurrence of intraclasts indicates rework erosion process of semi-consolidated sediments within the area of deposition. The penecontemporaneous deposits of weakly consolidated sediments were eroded from adjoining parts of sea bottom and redeposited as new

sediments. The erosion might be caused by storm waves or underwater slides (Folk, 1959).

6.5.7 Pellets

Pellets (Folk, 1959) are dominant in the Khao Khad area and common in the lower part of the Khao Chan area. They are found as dark grey bodies of rounded, spherical to elliptical aggregates of microcrystalline calcite ooze with devoid of any internal structure. They show uniform shape but variable sizes (40 to 120 μms). The pellets are a dominant constituent of recent subtidal and shallow intertidal coastal area. However, they occur preferentially in low-energy zones but can be transported without destruction even into high-energy environments if early intergranular cementation has taken place (Wetzel, 1937 cited in Flügel, 1982). A rapid cementation of fecal pellets is possible particularly in low-energy shallow-water areas supersaturated with $CaCO_3$ (Flügel, 1982).

6.5.8 Oncoids

Oncoids are irregular algal coated grains with calcareous cortex with partially overlapping algal laminae (Tucker et al., 1990). They are locally present in the unit KD2 in the lower part of Khao Khad area and as host grains of algal stromatolite. The presence of oncoids represents a morphological and ecological adaptation of encrusting organism in soft bottom and low-energy environments (Monty, 1974 and Peryt, 1975 cited in Flügel, 1982).

6.5.9 Micrite

Micrite (Folk, 1959) is found as groundmass or matrix of the fine-grained carbonate rocks which can be recognized partly through the sequence of the Khao Khad Formation. Petrographically, it can be recognized as subtranslucent, faint brownish grey, microcrystalline calcite crystals. The sizes of micrite grain vary from sub-microscopic grains up to 6 μms (it is however not greater than 4 μms based on Folk's definition). In hand specimen, it shows dull to opaque ultra-fine grained material having grey to black, greenish and brownish grey colors. It is probably designated as calcilutite in the field. It is noted that the micrite matrix can be found as gravitational sediment filling in the initial internal pore chamber of a fusulinid, known as geopetal sedimentary structure.

The elemental composition of 12 samples of micrite matrix is summarized in Table 6.4 and details in Appendix A. They show moderate concentrations of Fe, Mn, Na, K, Si and Ba respectively in degree of abundance. The Mg and Sr contents are below the detection limit of EPMA.

Table 6.4 Summary of trace element compositions of micrite matrix

	Elemental composition of micrite matrix (ppm)									
	Ca	Mg	Fe	Mn	Na	Sr	Ba	K	Si	Total
Min	381,789.16	0.00	0.00	0.00	0.00	0.00	0.00	0.00	0.00	382,872.82
Max	406,824.86	0.00	652.94	580.84	281.90	0.00	116.44	332.06	439.42	407,681.46
Average	393,407.09	0.00	254.57	134.24	95.20	0.00	32.84	89.93	54.15	394,068.03
SD	7,771.15	0.00	181.94	190.17	113.78	0.00	49.70	110.01	126.51	7,838.10

The micrite matrix in the Khao Khad formation was probably derived from skeletal debris which was broken down by bottom scavengers, boring algae and abrasion from wave and current action to form calcilutite. Local differences in

topography control sediment characteristic and distribution of calcarenite (with small patches of calcilutite) in low-lying area.

6.5.10 Calcite Cement

Calcite cement is generally forms as clear to slightly turbid calcite crystals of varying shapes and sizes (10 to 500 µms in diameter). It usually forms as pore-filling cement. The details of various types of calcite cement are described in the section of diagenetic processes.

6.6 Diagenetic Processes

The Permian carbonate sequences of the Khao Khad Formation have experienced many types of diagenetic alteration which overprinted and have obscured some of earlier sedimentary textures and structures. Those diagenetic alterations include grain abrasion, micritization, cementation, dolomitization, silicification, calcitization, dissolution, neomorphism and compaction. Such diagenetic processes produce various kinds of diagenetic textures which reflect a rather complex diagenetic history.

6.6.1 Grain Destruction and Bioturbations

Grain destruction and bioturbation are processes took place on carbonate sediments after deposition. The biological destruction process is commonly known as micritization. The mechanical destruction process is more active in high-energy zone where grain abrasion is generally slow but extensive. Both processes are active during early diagenesis. The bioturbation described here is burrow structures which are significantly found in the hand specimens and thin-sections.

6.6.1.1 Micritization

The micritization is a process of repeated micro-algal boring of carbonate skeletons leaving empty voids which later have been filled with micrite (Bathurst, 1966). Under a prolong influence of this process, carbonate grains were gradually and centripetally replaced by micrite. There are two products of diagenetic micritization observed under a microscope, namely, micritized grains and micrite envelopes that can be distinguished from micrite matrix. Various degree of micritization found throughout the Khao Khad Formation. The most common micritized grains are fusulinid skeletons and bryozoa fragments which were completely micritized. They are usually obscures the original rim and commonly show blur original internal structure (Figure 6.3A). Petrographically, micritized portion of bioclast is made up of microcrystalline calcite ranging in size from 2 to 6 μms in diameters. The tiny calcareous patches of 10 to 20 μms size occasionally associated with the microcrystalline calcite. The unaltered portion of bioclast usually shows light gray to dark gray in plane-polarized light. The micrite envelope is a dark color zone bound along the rim of any grain which does not collapse (Figure 6.3B). The most common micrite envelope is found in un-collapsed fusulinid fragments embedded in equant calcite cement. The micrite envelope was probably the result of incomplete micritization by which the centripetal micritization process did not progress into the inner portion of the grain or the process was terminated before the grain was completely micritized (Bathurst, 1971; Sibley and Murray, 1972).

The trace element composition of micritized grains (24 samples) are summarized in Table 6.5 and details in Appendix A. They contain moderate concentrations of Fe and Na, and low contents of Si, Mn, K, Ba and Mg. The Sr content is below the detection limit of EPMA.
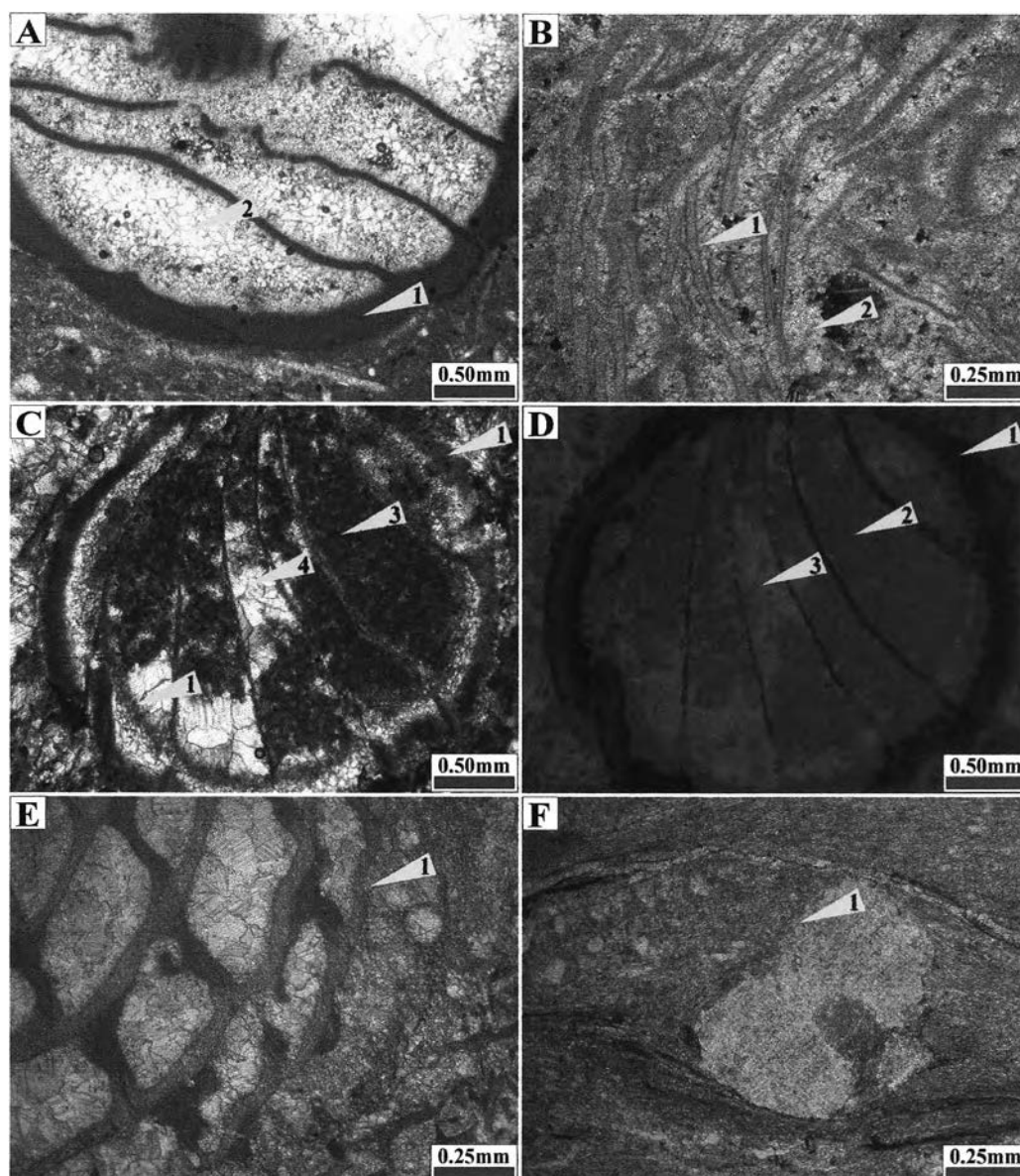
Figure 6.3 **A**: Photomicrograph of biosparudite showing a fusulinid shell was completely micritized (1) and obscures the original shell structure. The internal pore chambers were filled with equant calcite cement (2) (PPL); **B**: Photomicrograph of packed biomicrudite showing micrite envelopes (1) on shell surfaces before broken and cemented by equant calcite cements (2). (XPL); **C**: Photomicrograph of biosparudite showing micritized fusulinid shell (1) with microcrystalline calcite cement (2) lining internal pore surface. The internal pore chambers were filled by micrite (3) and blocky calcite cement (4). (PPL); **D**: Cathodoluminescence of C showing dull to non-luminescent micritized shell (1), dull luminescent micrite matrix (2) and bright luminescent blocky calcite cements (3). (CL); **E**: Photomicrograph of biosparudite with incomplete fusulinid shell (1) and small unidentified skeletons due to abrasion. (Stained, PPL); **F**: Photomicrograph of laminated biomicrite showing a crinoid fragment with straight edge (1), suggested the product of abrasion. (PPL)

Table 6.5 Summary of trace element compositions of micritized grains

| | Elemental composition of micritized grains (ppm) | | | | | | | | |
	Ca	Mg	Fe	Mn	Na	Sr	Ba	K	Si	Total
Min	383,690.24	0.00	0.00	0.00	0.00	0.00	0.00	0.00	0.00	384,320.16
Max	413,049.84	174.92	559.67	255.57	816.04	0.00	304.53	664.12	930.26	413,545.25
Average	397,373.64	7.29	228.66	63.89	202.77	0.00	53.37	62.95	89.99	398,082.56
SD	7,949.92	35.71	204.32	89.60	236.81	0.00	87.26	142.57	211.06	7,877.28

Under a cathodoluminoscope, micritized grains display both dull red and inert (Figures 6.3C and 6.3D). The dull red diagenetic micrite has similar luminescing appearance as those observed in micrite matrix and micrite filled in fusulinid chambers. The inert or non-luminescing diagenetic micrite is found as thin wall in certain grains, and as thick wall coating on the dull red luminescing micrite.

Interpretation: Micritization and micrite envelopes have been suggested to be caused by microbial boring by many authors (e.g. Bathurst, 1966; Friedman et al., 1971; Kobluk and Risk, 1977; Reid et al., 1992; Reid and Macintyre, 1998; Tucker, Wright and Dickson, 1990; and Reid and Macintyre, 2000). The original grains were bored around the rim by endolithic algae, fungi and bacteria and the bored holes were filled with fine-grained sediments or cement. The micrite envelopes could have been formed by the process as described above or by entrapping of fine sediments by micro-filaments and produced the micrite encrustation surrounding the grains. The intense activity of the endolithic microbe could cause completely micritized grains and the original skeletal nature might be difficult to determine (Tucker et al., 1990). These processes are very common in modern and fossil marine carbonate in intertidal environments and beach rocks (Meyers, 1987; Strasser et al., 1989; El Moursi and Montaggioni, 1994). However, they are also observed in subtidal environment in the Paris Basin (Purser, 1969) and Pleistocene Atlantic shelf (Friedman et al., 1971). Micritization has also occurred to some degree in most shallow marine environments,

but it is particularly predominant in quiet carbonate platform interior within photic zone (Bathurst, 1966). Macintyre and Reid (1995, 1998) studied recrystallization in calcareous algae and foraminifera living on the seafloor and reported syndepositional recrystallization involving textural change to be pseudomicrite and minimicrite. Reid and Macintyre (1998, 2000) reported carbonate recrystallization in shallow marine environments as a widespread diagenetic process forming micritized grains. It is concluded that the skeletal fragments were micritized in the intertidal to subtidal environments of shallow marine with empty internal pore before the development of marine cements. The presence of non-luminescence coated on dull luminescence in the thick micritized shell indicates that the inner part of micritized shell was original shell structure and the outer part was the early cement occurred in oxidizing condition. The presence of micrite envelope on fusulinid shell surfaces except at the end of broken fragments in coarse spar calcite cement indicates that the micrite envelopes developed before grains were broken.

6.6.1.2 Grain Abrasion

Grain abrasion can be easily recognized on crinoid grains and fusulinid tests. They are usually found as rounded grains with incomplete outline of original grain. Most of allochthonous allochems were affected by various degree of grain abrasion. They can be observed throughout sedimentary sequence of the Khao Khad Formation. Grain abrasion is the product of physical processes acting upon carbonate sediments during early deposition. The major physical processes are tidal current and wave actions initiating grain movement or transport, especially in the high energy zones, such as intertidal and barrier bar. During grain movement or transportation, they were collided with each others and with hardground surface that could scratch and abrade outer rim of grains. These processes can reduce the size of allochem and destroy the original structure of the grain surface. Some fusulinid shell fragments show incomplete

convolute structure in which the rims were abraded (Figure 6.3E). Most crinoid fragments also show abraded and flattened rims (Figure 6.3F).

Interpretation: These features indicate that the grains were deposited and undergone the processes of agitation or transportation in a zone of high-energy environment, such as intertidal and barrier bar. The skeletal debris was further broken down by abrasion from wave and current action.

6.6.1.3 Burrows

Burrows in the Khao Khad Formation are found in the unit KD5, KD7, PK2 and PK3. They consist of one large tabular burrow (2 to 5 mms across, Figure 6.4A) crosscut by two different smaller burrows (Figure 6.4B). They are filled by various types of materials in each unit. In the unit KD5, burrows were found in micrite matrix and filled by pelmicrite and equant sparry calcite (Figure 6.4C). In the Unit KD7, burrows were also found in dark color micrite matrix and filled by light color micrite as geopetal structure and subsequently by microcrystalline dolomite, mesocrystalline dolomite and cemented by sparry calcite (Figure 6.4D). The microcrystalline dolomite forms as subhedral to euhedral crystals varying from 6 to 30 μms in size and the mesocrystalline dolomite is euhedral crystals of 30 – 60 μms in size. The burrows in the unit PK2 were repeated bores varying in sizes and shapes. They were filled with micrite as geopetal structure, pellets and micrite, microcrystalline dolomite and sparry calcite cement (Figure 6.4E). Burrows in the unit PK3 were partially filled by micrite and interstices were filled by equant calcite cement (Figure 6.4F).

Interpretation: Burrowing organisms are active in the fine-grained carbonate sediment deposited in intertidal and subtidal environments (Seilacher, 1978 and Flügel, 1982). The presence of burrows therefore indicate that the fine-grained sediments were
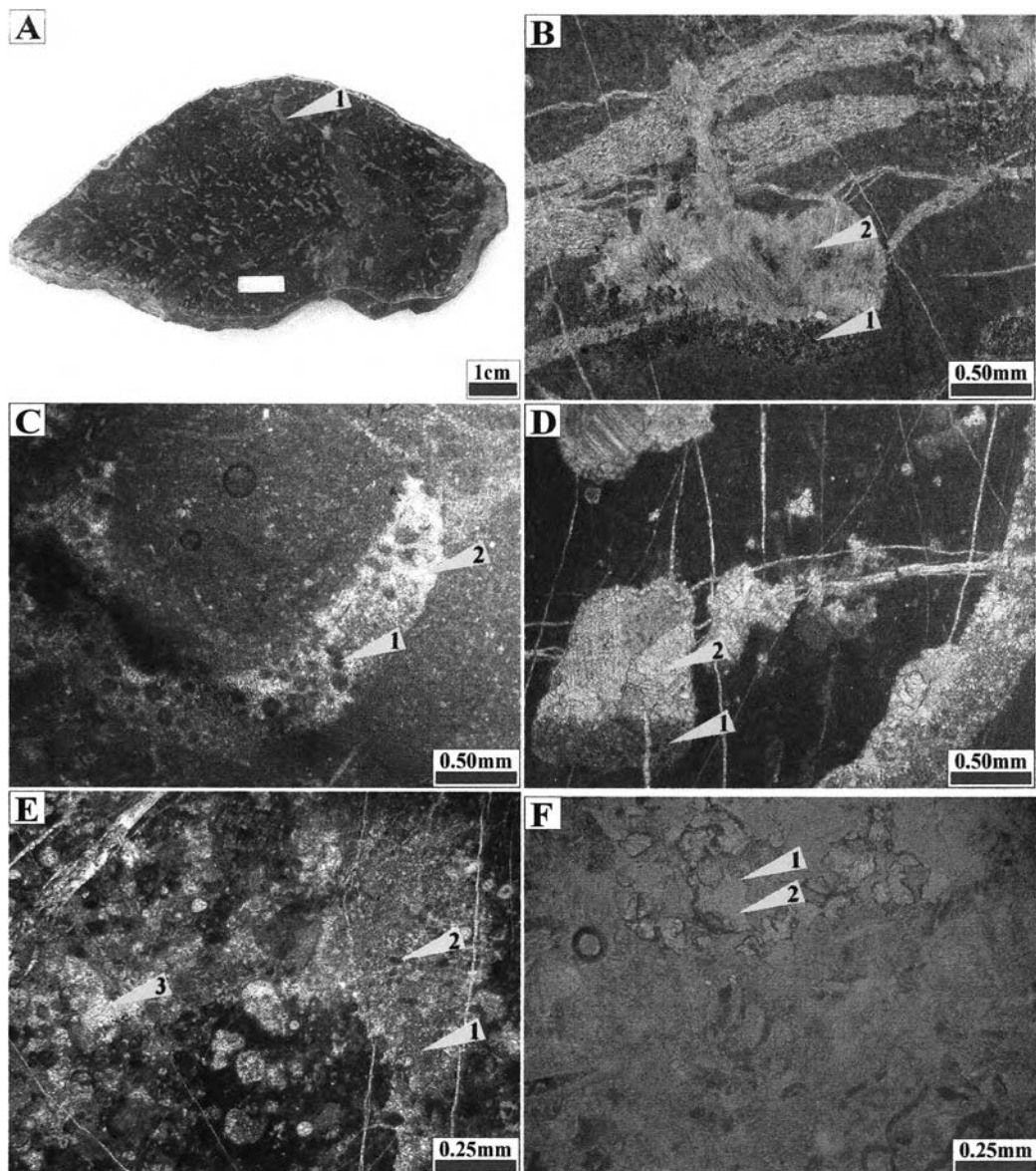
Figure 6.4 **A**: A dismicrite slab with abundant burrows (1).; **B**: Photomicrograph of burrows filled with mesodolomite (1) and the void remain occluded by blocky calcite cement (2). (Stained, PPL); **C**: Photomicrograph of burrow in dismicrite filled with pelmicrite (1) and sparry calcite cement (2). (PPL); **D**: Photomicrograph of burrow filled with microdolomite (1) and blocky calcite cement (2). (PPL); **E**: Photomicrograph of burrow filled with micrite (1), pelmicrite (2) and blocky calcite cement (3). (Stained, PPL); **F**: Photomicrograph of burrows (1) in biosparite filled with sparry calcite (2). (Stained, PPL)

deposited in the intertidal to subtidal environments where burrowing was active. Later on, the burrows were partially filled by micrite matrix, fecal pellets, microcrystalline and mesocrystalline dolomites and sparry calcite cement, sequentially.

6.6.2 Meniscus Cementation

Meniscus cement is defined as micrite precipitating around grain surfaces and a pore-rounding habit. Occasionally, it locates near grain contact where they have grown to conform to the air-water interface showing concave-like surfaces in the cross-sections. It is associated with micrite envelope in the unit KD4 (Figure 6.5A). Petrographically, the meniscus cement is dark color micrite similar to micrite envelope and micrite matrix filled as geopetal structure in shell. But, their distinctive features of double concave boundary between grain contact areas make it easy to recognize.

Interpretation: The meniscus cement has been interpreted as vadose cement due to the droplets hold by capillary force in pores partly filled by air (Dunham, 1971; and Longman, 1980). Such features were interpreted to occur in intertidal environment (Mayers, 1987; Bernier and Dalongeville, 1988; and El Moursi and Montaggioni, 1994). In modern carbonates, the micrite cement has been found in many areas in the form of high magnesium calcite cement in beach rock (Friedman, 1964, 1968). So, it is likely that the meniscus cement found in the unit KD4 indicates the intertidal environment.
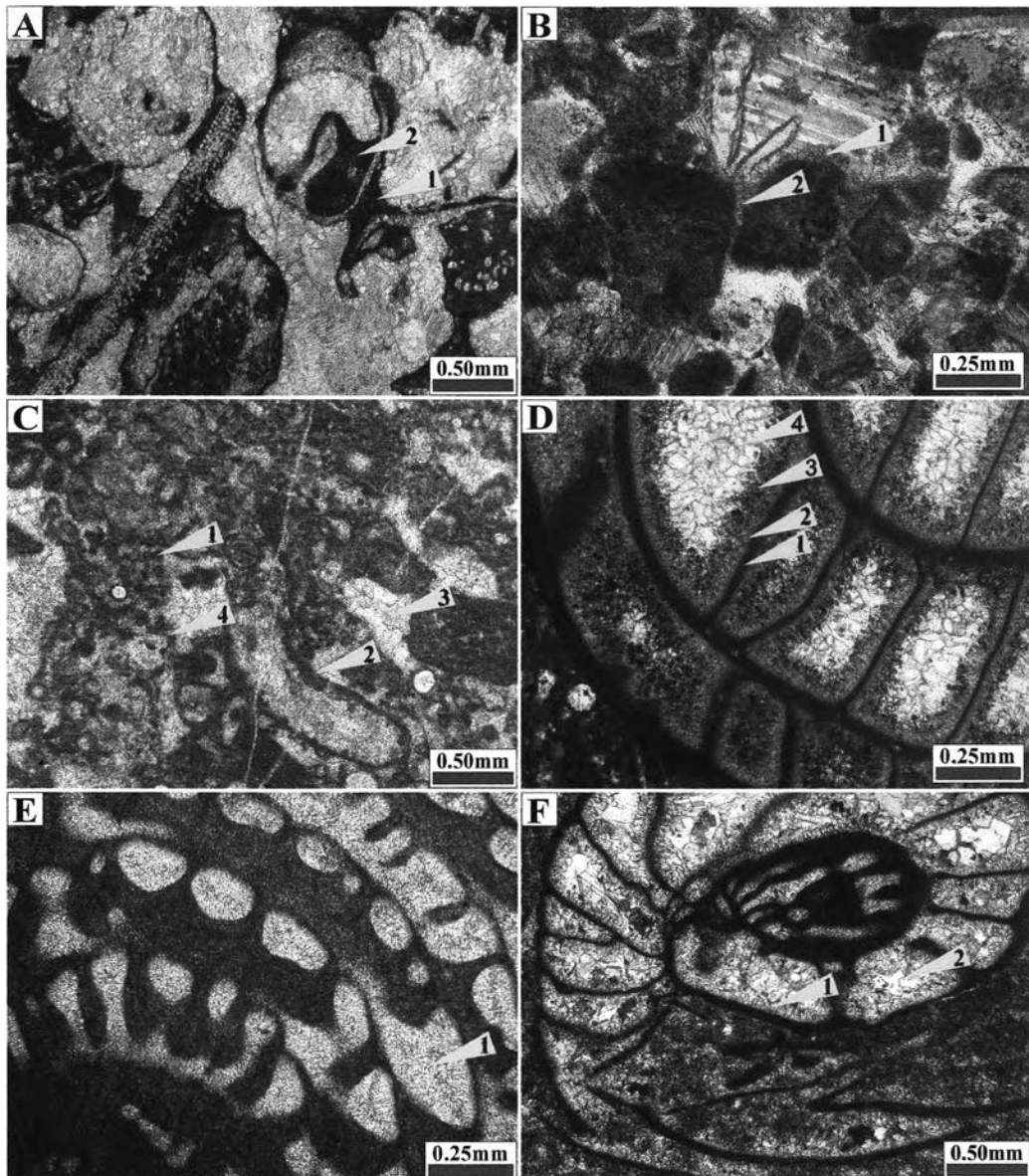
Figure 6.5 **A**: Photomicrograph showing meniscus cement (1) at contact point of grains and some micrite filled (2) as geopetal structure in internal pore space. (PPL); **B**: Photomicrograph of biosparite showing microcrystalline calcite cement around micritized grains (1) and contact point of grains (2). (PPL); **C**: Photomicrograph of biopelsparite showing abundant pellet (1) and micrite-enveloped bioclasts (2) cemented by sparry calcite (3). The pellets were initially cemented by microcrystalline calcite cement (4). (PPL); **D**: Photomicrograph showing sequence of cements in the internal pore space of micritized fusulinid test (1). The acicular fibrous calcite cement (2) fringed around the internal pore surface and followed by micrite filled (3). The pore remains were occluded by equant calcite cement (4). (PPL); **E**: Photomicrograph showing acicular fibrous calcite cement (1) occluded the internal pore space of fusulinid test. (PPL); **F**: Photomicrograph showing abundant dog-tooth calcite cement (1) grown on the surface of micritized fusulinid shell and followed by equant calcite (2). (XPL)

6.6.3 Calcite Cementation

Petrographical observation reveals seven fabrics of calcite cement, namely, microcrystalline calcite cement, acicular fibrous cement, dog-tooth calcite cement, radiaxial fibrous cement, syntaxial overgrowths calcite cement, equant calcite cement and blocky calcite cement.

6.6.3.1 Microcrystalline Calcite Cement

The microcrystalline calcite cement is composed of 4 to 10 μms sized crystals of calcite encrusted on grain surface (Figure 6.5B). This type of cementation is generally clearer in color and coarser in grain size than those of the micrite envelopes, the micritized grains and micrite matrix. The cement usually occurs around grain surface or on dissolution surface at about 10 to 20 μms thick. It is also found around a grain-to-grain contact point and commonly found as early cement in pelsparite (Figure 6.5C).

The trace element compositions of microcrystalline calcite cement (14 samples) are summarized in Table 6.6 and details in Appendix A. The graphic plot of trace element in calcite cement is shown in Figure 6.6. They contain low concentrations of Na, Fe, Mn, Ba, K and Si. The Mg and Sr contents are below the detection limited of the EPMA. The luminescence of microcrystalline calcite cement is dull similar to micrite matrix invading shell chamber (Figures 6.3C and 6.3D).

Interpretation: The microcrystalline calcite cement has been group as a type of micrite cement by many authors (Thorstenson et al., 1972; Moore, 1973; James et al., 1976; Land and Moore, 1980; Flügel, 1982; Jindrich, 1983; Marshall, 1983; Mayers, 1987; Tucker et al., 1990). The micrite cement is a characteristic cementation in intertidal to subtidal setting which represents μm-sized crystals occurring as abundant
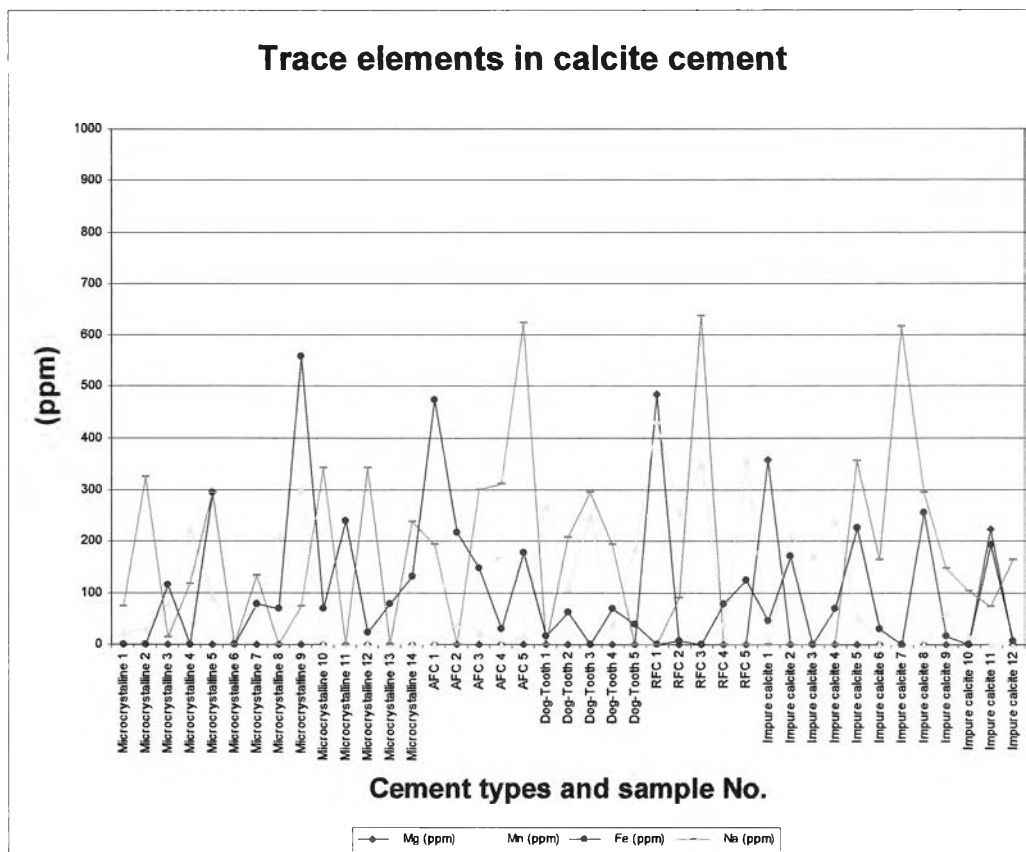
Figure 6.6 Graphic plot of 4 trace element contents in the microcrystalline calcite cement, acicular fibrous calcite cement (AFC), dog-tooth calcite cement, radiaxial fibrous calcite cement (RFC) and impure equant calcite cement.

rim cement and grain contact cement. However, the present study differentiates the microcrystalline calcite cement from micrite cement due to the difference in crystal size, color, clarity and location related to other fabrics. Mayers (1987) also categorized microcrystalline calcite from micrite cement and reported that it occurred in marine vadose zone on the beach in Hawaii. The presence of microcrystalline calcite cement around the dissolution surface and around the grain contact point is a good indication that the sediments were cemented in the marine vadose zone.

Table 6.6 Summary of trace element composition of microcrystalline calcite cement

	Elemental composition of microcrystalline calcite cement (ppm)									
	Ca	Mg	Fe	Mn	Na	Sr	Ba	K	Si	Total
Min	379,773.72	0.00	0.00	0.00	0.00	0.00	0.00	0.00	0.00	380,759.42
Max	407,796.85	0.00	559.67	302.04	341.25	0.00	438.88	265.65	168.29	408,027.00
Average	388,751.80	0.00	113.82	74.13	139.89	0.00	45.42	33.21	36.73	389,200.00
SD	7,398.00	0.00	155.51	100.23	139.51	0.00	120.34	69.84	52.91	7,354.52

6.6.3.2 Acicular Fibrous Cement

Acicular fibrous cement usually fringes around the grain surface as well as lining internal chambers of fusulinid shells (Figures 6.5D and 6.5E). This type of cementation is found in the interstices of bioclasts in the unit KD3 and KD6. The crystals of the acicular cement are very small ranging in size from 3-6 μms wide and 30-50 μms long.

The trace element compositions of acicular fibrous calcite cement (5 samples) are summarized in Table 6.7 and details in Appendix A. They contain moderate concentrations of Na and Fe and low contents of Ba, K, and Mn. The Mg, Sr and Si contents are lower than the detection limit of EPMA.

Table 6.7 Summary of trace element compositions of acicular fibrous calcite cement

	Elemental composition of acicular fibrous calcite cement (ppm)								
	Ca	Mg	Fe	Mn	Na	Sr	Ba	K	Si	Total
Min	383,332.90	0.00	31.09	0.00	0.00	0.00	0.00	0.00	0.00	386,157.90
Max	398,555.86	0.00	474.16	38.72	2,299.74	0.00	304.53	132.82	0.00	398,812.23
Average	392,413.79	0.00	209.87	15.49	685.47	0.00	60.91	39.85	0.00	393,425.38
SD	6,187.34	0.00	163.33	16.43	930.33	0.00	136.19	55.81	0.00	5,376.88

Cathodoluminescence of acicular fibrous calcite cement is dull red similar to those of the inner part of micritized shells.

Interpretation: The acicular fibrous cement was formerly acicular aragonite cement, which was precipitated in recent carbonate sediments under very shallow hypersaline marine water where CO_2 was easily expelled (Friedman, 1968; Tucker et al., 1990). Similar style of acicular fibrous aragonite cement was reported in recent marine sands (Given and Wilkinson, 1985). During diagenesis this aragonite cement could paramorphically transformed to low magnesian calcite by which its original depositional fabric was still preserved (Baird, 1992). As a result this acicular fibrous calcite cement was probably the earliest phases of marine cementation under very shallow hypersaline environment. It originally precipitated as acicular fibrous aragonite cement then was replaced by calcite

6.6.3.3 Dog-tooth Calcite Cement

The dog-tooth calcite cement is found as an early phase of calcite cement fringing around the surface of inter- and intragranular pore spaces of the unit KD3, KC1, KC4, KC9, PK1 and PK3 (Figures 6.5F and 6.7A). This type of cementation is characterized by sharply pointed crystal of acute scalenohedral calcite crystals grown
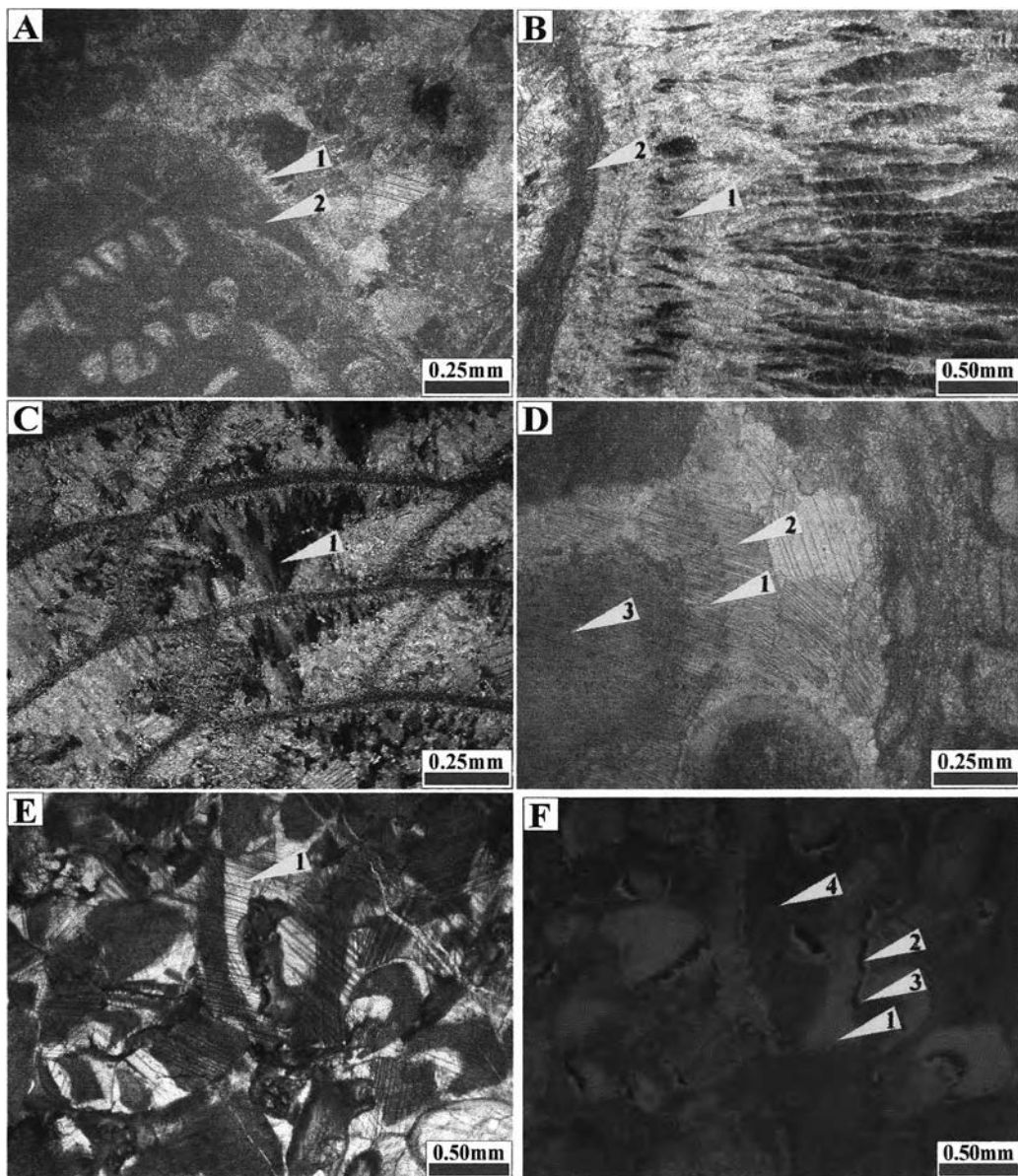
Figure 6.7 **A**: Photomicrograph of biosparite showing abundant dog-tooth calcite(1) cement grew in upright position on the micritized grain surface (2), lining the intergranular pore space. (XPL); **B**: Photomicrograph of radiaxial fibrous calcite cement (1) grew on algal coated stromatolite (2), occluded the intergranular pore space. (XPL); **C**: Photomicrograph of radiaxial fibrous calcite cement (1) occluded the internal pore space of fusulinid test. (XPL); **D**: Photomicrograph of crinoidal biosparite showing at least two generations of syntaxial overgrowth calcite cement (1, 2) on the crinoid grain (3). (XPL); **E**: Photomicrograph of crinoidal biosparite showing the intergranular pore space was completely occluded by syntaxial overgrowth calcite cement (1). (PPL); **F**: Cathodoluminescence of E showing comparatively bright red luminescence of original crinoid fragments (1). The syntaxial overgrowths calcite cements showing initially non-luminescence zone (2) and followed by bright red luminescence zone (3). It is noted that the matrix is dull luminescence (4) of former micrite matrix. (CL)

in upright position fringing around the pore surface. The crystals vary from 10 - 40 µms wide and 30 - 100 µms long.

The trace element compositions of dog-tooth calcite cement (5 samples) are summarized in Table 6.8 and details in Appendix A. They contain moderate concentrations of K, Mn, Na and Si, and low contents of Fe, Ba and Si. The Mg, and Sr contents are below the detection limit of EPMA.

Table 6.8 summary of trace element compositions of dog-tooth calcite cement

	Elemental composition of dog-tooth calcite cement (ppm)									
	Ca	Mg	Fe	Mn	Na	Sr	Ba	K	Si	Total
Min	407,603.88	0.00	0.00	38.72	0.00	0.00	0.00	99.62	0.00	408,089.24
Max	412,056.42	0.00	69.96	271.06	296.74	0.00	71.65	265.65	65.45	412,795.42
Average	409,093.30	0.00	37.31	170.38	139.47	0.00	23.29	175.99	17.76	409,657.50
SD	1,783.12	0.00	29.80	96.88	133.37	0.00	33.27	64.94	28.51	1,846.85

Interpretation: The dog-tooth calcite cement has been reported as early marine cements, however, some authors interpreted as fresh water cement. Khantaprab (1972) studied the diagenesis of quaternary limestones from the Persian Gulf and found abundant dog-tooth calcite cement, of low magnesian type grew in the intra-particle pore spaces in the shallow burial carbonate sediments. The presence of some dog-tooth calcite cement fringing around the pore surfaces should also occurred in the shallow burial marine environment.

6.6.3.4 Radiaxial Fibrous Calcite Cement

The radiaxial fibrous calcite cement is a common pore-filling fabric in ancient limestones and is defined by a distinctive combination of curved twins within single crystal (Bathurst, 1959; Davies, 1977; Lohmann and Meyers, 1977; Mattes and

Mountjoy, 1980; and Saller, 1986). In the Khao Khad Formation, the radiaxial fibrous calcite cement appears as turbid elongate crystals isopachous rind in the intergranular and intragranular pore spaces. It is found in the unit KD2, KD6, PK2 and PK3. Rinds are typically 50-200 μms thick, but can be as thin as 10 μms and as thick as 500 μms. In part of the unit KD2, the radiaxial fibrous calcite cement occludes the intergranular pore spaces of algal stromatolite (Figure 6.7B). It was firstly precipitated as small druse fibrous calcite cement around stromatolite surfaces, occasionally, associated with microcrystalline and mesocrystalline dolomite. There are at least three generations of radiaxial fibrous calcite cement precipitated over the stromatolite layer and each separated by layers of microcrystalline and mesocrystalline dolomite. The crystals sizes are gradually increase toward pore center. The crystals of radiaxial fibrous calcite are turbid, curve cleavage, and show wavy extinction. The rest of the intergranular pores were filled by equant calcite cement, partly, and macrocrystalline dolomite. In part of the unit KD6, PK2 and PK3 the radiaxial fibrous calcite cement appear associate with fusulinid tests. They are firstly precipitated as druse fibrous cement around inter- and intragranular pore of fusulinid tests. No spirotheca has been observed in inner shell chambers (Figure 6.7C). The radiaxial fibrous cement grows optical continuity outward from the druse rimed cements. The enfacial junction of radiaxial fibrous calcite is triangular.

The trace element compositions of the radiaxial fibrous calcite cement (5 samples) are summarized in Table 6.9 and details in Appendix A. They contain high concentrations of Mg, Mn, K and Na, and some contents of Fe, Ba and Si. The Sr content is below the detection limit of EPMA.

Table 6.9 Summary of trace element compositions of radiaxial fibrous calcite cement

	Elemental composition of radiaxial fibrous calcite cement (ppm)									
	Ca	Mg	Fe	Mn	Na	Sr	Ba	K	Si	Total
Min	379,402.08	0.00	0.00	38.72	0.00	0.00	0.00	33.21	0.00	382,647.89
Max	406,174.49	2,485.08	124.37	433.70	637.99	0.00	125.39	315.46	28.05	406,742.70
Average	398,803.15	497.02	41.97	286.55	145.40	0.00	34.04	232.44	5.61	400,046.18
SD	11,274.94	1,111.36	56.48	152.26	278.05	0.00	54.63	118.57	12.54	10,087.00

Interpretation: The origin of radiaxial fibrous calcite cement, which is a common pore filling fabric in ancient carbonate rocks, has been discussed in the literatures as either marine replacement or burial cement (e.g. Kendall and Tucker, 1973; Longmann and Meyers, 1977; Mattes and Mountjoy, 1980; Kendall, 1985; Seller, 1986; Tucker et al., 1990; Mazzullo et al., 1990; Reinhold, 1998; and Kim and Lee, 2003). Kendall and Tucker (1973) suggested that radiaxial fibrous calcite cement have been modified from acicular high magnesian calcite which precipitated from normal marine agitated water. The turbid crystals of radiaxial fibrous calcite have been suggested to be caused by the presence of microcrystalline dolomite (Lohmann and Mayer, 1977), organic material and other solid impurities (Kendal and Tucker, 1973), or fluid filled micro-cavities (Kendall, 1985; Seller, 1986). Based on the inclusion within crystals, the radiaxial fibrous calcite in the unit KD2 contains abundant both microcrystalline and mesocrystalline dolomite. However, there are slightly few unidentified turbid inclusions in the other unit. The presence of microcrystalline dolomite precipitated in calcite crystal was suggested to occur in the area of low water/rocks ratio (Tucker et al., 1990) or they were originally composed of magnesian calcite and converted to low magnesian calcite as incongruent dissolution (Land, 1967; Bathurst, 1971). The data from EPMA shows that they contain slightly high magnesium content than adjacent grains or sparry calcite cement. During the diagenesis, the high magnesian calcite may lose Mg^{2+}, but they may still retain sufficient to indicate an original high level (Marshall and Ashton, 1980;

Prezbindowski, 1985; Tucker et al., 1990). It concludes that the radiaxial fibrous cement replaced the former acicular high magnesian calcite in shallow marine environment. Tittirananda (1976) and Wongwanich (1990) also proposed a marine origin for similar radiaxial fibrous calcite cement of the Permian Ratburi limestone in central Thailand and Ordovician Thung Song carbonate in southern Thailand, respectively.

6.6.3.5 Syntaxial Overgrowth Calcite Cement

The syntaxial overgrowth calcite cements are common in the unit KC2, KC3, KC4, KC6, KC8 and KC9. They form as overgrowths on crinoid fragments in the poorly- washed biosparite and biosparite. The overgrowth cements have developed in optical continuity with single crystalline host grains. The thicknesses of overgrowth vary from few μms to several hundred μms extending outward into interstices. At least two stages of overgrowths have been observed on a single grain (Figure 6.7D). They postdated the micritization, micrite envelopes and the microcrystalline calcite cement. Under a cathodoluminoscope, the overgrowths show zones of luminescence resulting from different phases of precipitation (Figures 6.7E and 6.7F). It appears that most original grains are rounded rim and show moderately red luminescence embedded in dull luminescent matrix. Some crinoid grains show mottled, small dull luminescent. The overgrowth shows at least two zones of luminescence, non-luminescence and bright luminescence. The non-luminescence zone is the first phase of overgrowth cement growing as saw tooth rim on the side of grain in the direction of c axis. The second phase of overgrowth cement is bright luminescence and grows on the non-luminescence zone with sharp boundary. There are many sub-zones in the second phase. Some overgrowth zones show a remnant of partial dissolution before re-precipitation (Figures 6.8A and 6.8B). Many bright and dull sub-zones follow the dissolution surface as well as overgrowth cements.
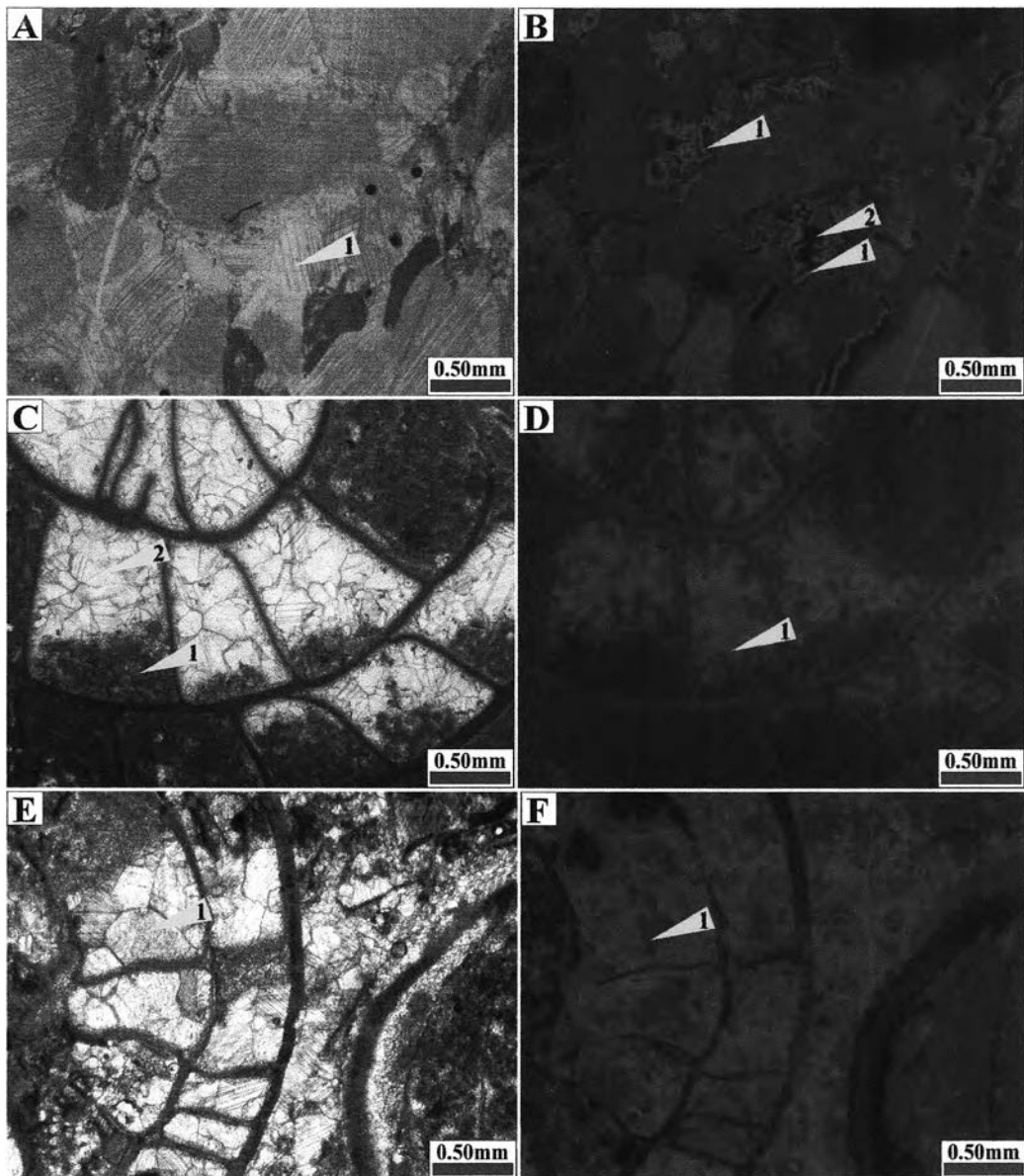
Figure 6.8 **A**: Photomicrograph of crinoidal biosparite which the intergranular pore
space were occluded by syntaxial overgrowth calcite cement (1). (PPL);
B: Cathodoluminescence of A showing parallel zoning (1) of luminescence
lining on the dissolve surface of intergranular pores (2). (CL); **C**:
Photomicrograph of biomicrudite showing some micrite filled (1) as geopetal
structure in fusulinid chambers and cemented by equant calcite (2). (PPL); **D**:
Cathodoluminescence of C showing parallel zoned crystals (1) of equant
calcite cement. (CL); **E**: Photomicrograph of biosparudite showing impure
blocky calcite cement (1) filled both inter- and intragranular pore space.
(PPL); **F**: Cathodoluminescence of E showing non-parallel zoned crystals (1)
of blocky calcite cement. (CL)

The trace element compositions of syntaxial overgrowth calcite cement (38 samples) are plotted in Table 6.10 and Figure 6.9 and details are in Appendix A. They contain high concentrations of Fe, moderate contents of Mn and Na, and low K and Mg contents. It reveals that concentration of Fe decreases through the scan line from inner to outer zones of overgrowths cement (e.g. line-scan C1-C2, D1-D5, E1-E3, J1-J4 and L1-L3). However, some overgrowths started with low Fe content (e.g. line-scan I1-I2 and K1-K3). The concentration of Mn also varies and seems antipathetic to Fe content.

Table 6.10 Summary of trace element compositions of syntaxial overgrowths calcite cement.

| | Elemental composition of syntaxial overgrowth calcite cement (ppm) | | | | | | | | | |
	Ca	Mg	Fe	Mn	Na	Sr	Ba	K	Si	Total
Min	385,348.33	0.00	0.00	0.00	0.00	0.00	0.00	0.00	0.00	385,532.44
Max	419,660.76	506.98	1,507.99	743.48	1,083.10	0.00	152.26	265.65	313.20	420,404.25
Average	405,873.01	23.65	488.68	178.13	155.01	0.00	17.68	51.56	31.74	406,819.45
SD	8,919.76	98.01	355.09	154.05	201.34	0.00	38.14	63.05	68.31	8,936.35

Interpretation: The syntaxial overgrowth is common cement in biosparite and its origin has been extensively discussed. Many ancient carbonates contain abundant syntaxial overgrowths on crinoids. The overgrowths were interpreted as passive cement filling in original intergranular pores (Evamy and Shearman, 1965, 1969; Freeman, 1971; and Meyers, 1974, 1978). However, the overgrowths have also been reported to occur in muddy or micrite limestone lacking of original intergranular pores (Bathurst, 1975; Walkden and Berry, 1984; Braithwaite and Heath, 1989). Therefore the process of passive cement filling could not be accounted for the growing of all overgrowth cements. Bathurst (1975) proposed that the overgrowth was a neomorphic replacement of micrite by simultaneous dissolution and reprecipitation across thin solution film. In contrast, Walkden and Berry (1984) believed that it could occur by
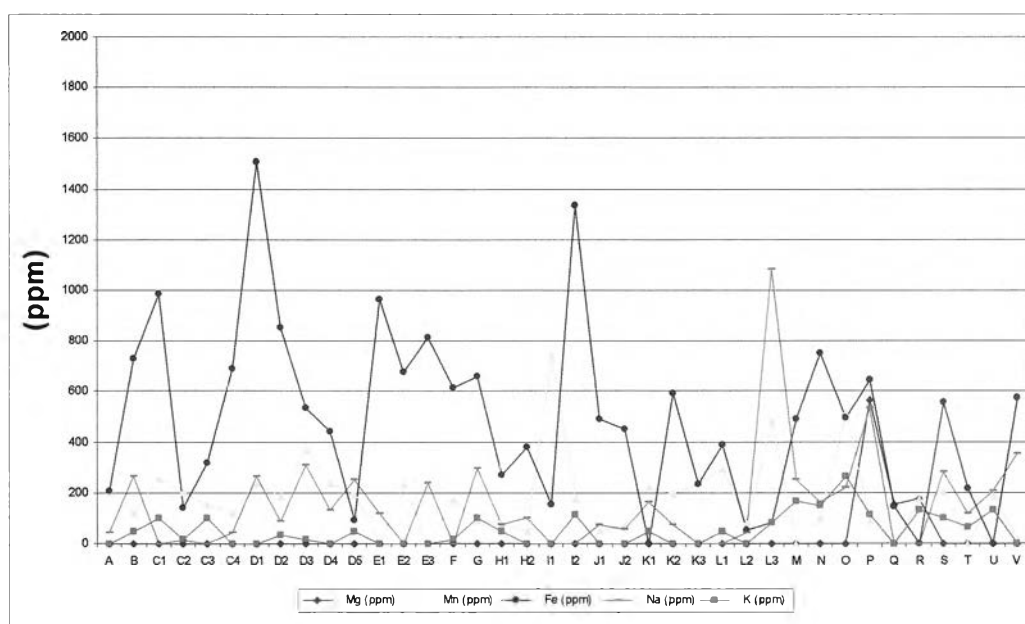
Figure 6.9 Graphic plot of line-scanning of 4 trace elements contents of syntaxial overgrowth calcite cement.

the process of solution corona. This process could occur in near-surface condition producing non-luminescence and might be ended in burial condition where very bright luminescence was generated. The non-luminescence overgrowth cement indicated the precipitation under oxidizing marine condition (Wongwanich, 1990). The zoned luminescence overgrowths of the late stage favored the reducing environment of burial diagenesis (Meyers, 1974; Grover and Read, 1983). It was confirmed by Braithwaite and Heath (1989) that the overgrowths could be a displacive calcite precipitated in near-surface diagenesis. James and Choquette (1983) studied the sea-floor diagenesis and concluded that the syntaxial overgrowths of Mg-calcite on echinoderm particles were common phenomena in the shallow environment of ancient rocks.

From the above discussion, it was therefore likely that crinoids and associated allochems in the Khao Khad Formation were deposited together with micrite matrix before syntaxial overgrowth calcite cement was formed in shallow marine environment. The syntaxial overgrowth calcite cement initially precipitated in oxic condition, the late overgrowths developed from a restricted (or closed system) pore fluid in anoxic condition of restricted pore fluid.

6.6.3.6 Equant Calcite Cement

The equant calcite cement is rare in the Khao Khad Formation. It is found only as intragranular pore filling of biomicrite and biomicrudite of the unit KD6, KC1, KC4, PK1 and PK3. The crystal sizes usually vary from 5 to 30 μms and up to 200 μms in some parts. The cementing calcite crystals increase in size from the pore surface toward the center of the pore space. The crystals grow as irregular isopachous crust on the grains surface. They show interlock mosaic with compromise boundaries and triple enfacial junction. The equant calcite occurs as cement occluding internal chambers of fusulinid shells and corals, and fills intergranular pores.

Under a cathodoluminoscope, the equant calcite cement exhibits parallel zoned crystals (Figures 6.8C and 6.8D). The parallel zoning suggests the crystal growing from the pore surface toward the center.

The trace element compositions of equant calcite cement (29 samples) are plotted in Table 6.11 and details are in Appendix A. They contain moderate contents of Mn, Na, Fe and low contents of Ba, K and Si. The Sr and Mg content are below the detection limit of EPMA.

Table 6.11 Summary of trace element compositions of equant calcite cement

	Elemental composition of equant calcite cement (ppm)									
	Ca	Mg	Fe	Mn	Na	Sr	Ba	K	Si	Total
Min	390,772.85	0.00	0.00	0.00	0.00	0.00	0.00	0.00	0.00	390,772.85
Max	418,931.77	0.00	629.62	573.10	489.62	0.00	358.27	348.66	537.59	419,664.23
Average	401,231.11	0.00	101.61	165.40	138.30	0.00	58.54	36.17	31.39	401,762.52
SD	7,699.54	0.00	165.68	158.71	161.78	0.00	85.13	68.09	109.36	7,680.53

Interpretation: The presence of parallel zoned crystals under the cathodoluminoscope suggests that the equant calcite was precipitated from a closed system pore fluid of presumably burial condition. The collapse of micrite enveloped shells before the formation of equant calcite cement also confirms burial origin.

6.6.3.7 Blocky Calcite Cement

The blocky calcite cement is the most abundant cementation in the carbonate rocks in the study area. It occurs widespread and affects all units. They appear as sparry calcite mosaic, clear colorless crystals ranging in size from 10 to 500 μms filling both inter- and intragranular pore remains. The crystals usually increase in size from the pore surface toward the pore center. They show interlocking mosaic with

compromise boundaries and triple enfacial junction. The blocky calcite usually cements various fabrics such as infilling previous aragonite allochems, filling the pore remains in burrow and filling intergranular pores.

The blocky calcite cement is the most abundant cement types. The luminescent characteristic of this blocky calcite cement appears as sub-crystal aggregate within a single crystal (Figures 6.8E and 6.8F). Each crystal luminesces differently from bright to dull red.

The trace element compositions of blocky calcite cement (59 samples) are summarized in Table 6.12 and details are in Appendix A. They contain high concentrations of Mn, moderate contents of Na, and Fe and low contents of Ba, K and Si. The Sr and Mg content are below the detection limit of EPMA.

Table 6.12 Summary of trace element compositions of blocky calcite cement

	Elemental composition of blocky calcite cement (ppm)									
	Ca	Mg	Fe	Mn	Na	Sr	Ba	K	Si	Total
Min	380,131.07	0.00	0.00	0.00	0.00	0.00	0.00	0.00	0.00	380,819.99
Max	419,710.78	0.00	715.13	782.20	504.46	0.00	277.66	348.66	32.72	419,726.33
Average	392,245.12	0.00	191.00	250.59	132.47	0.00	31.35	96.06	9.02	392,955.61
SD	10,236.11	0.00	184.92	287.48	168.21	0.00	76.71	128.96	10.76	10,060.20

Interpretation: The blocky calcite cement can occur in a variety of environments, from fresh water (Friedman, 1964, 1968), shallow marine (Peirson and Shinn, 1985), near surface (Chafetz et al., 1985), to deep burial (Niemann and Read, 1988). However, the texture of small crystal aggregate within a large single crystal as revealed by cathodoluminoscope suggest that they occurred by the replacement pre-existing cement and probably retained their original trace element composition during burial diagenesis. It is concluded that the blocky calcite cement occurred in burial marine condition.

6.6.4 Dolomitization

Three types of dolomite have been recognized based on the differences in crystal size, morphology and relationship to other diagenetic fabrics. They include microcrystalline, mesocrystalline and macrocrystalline dolomites. They are found throughout the Khao Khad Formation except in the unit KD8, KD9 and KC8.

The trace element analyses of dolomite show low Fe and significantly high Na contents in the microcrystalline and mesocrystalline dolomites whereas significantly high Fe and low Na contents are found in the macrocrystalline and ferroan dolomites. The macrocrystalline dolomite contains more Mn content than the microcrystalline and mesocrystalline dolomites. The K values are not significantly different in all types of dolomite. (Figure 6.10)

6.6.4.1 Microcrystalline Dolomite

The microcrystalline dolomite forms as anhedral to subhedral crystals of a few μms in size (normally less than 10 μms). It is commonly found in the unit KD1, KD2, KD3, KD7, KC1, KC3, KC5, KC6, KC7, PK2 and PK3. This type of dolomite is usually occurred in association with dissolution surface, radiaxial fibrous calcite cement, burrows and microcrystalline quartz. In part of crinoidal biosparite, it is recognized as unstained microcrystalline crystals coated on the dissolution surface of pre-existing grains and cements (Figure 6.11A). The thin bands of microcrystalline dolomite are also found between layers of radiaxial fibrous calcite cement in algal stromatolite. In silicified limestones, microcrystalline dolomite appears disseminated in microcrystalline quartz matrix. Burrows are also filled with microcrystalline dolomite.
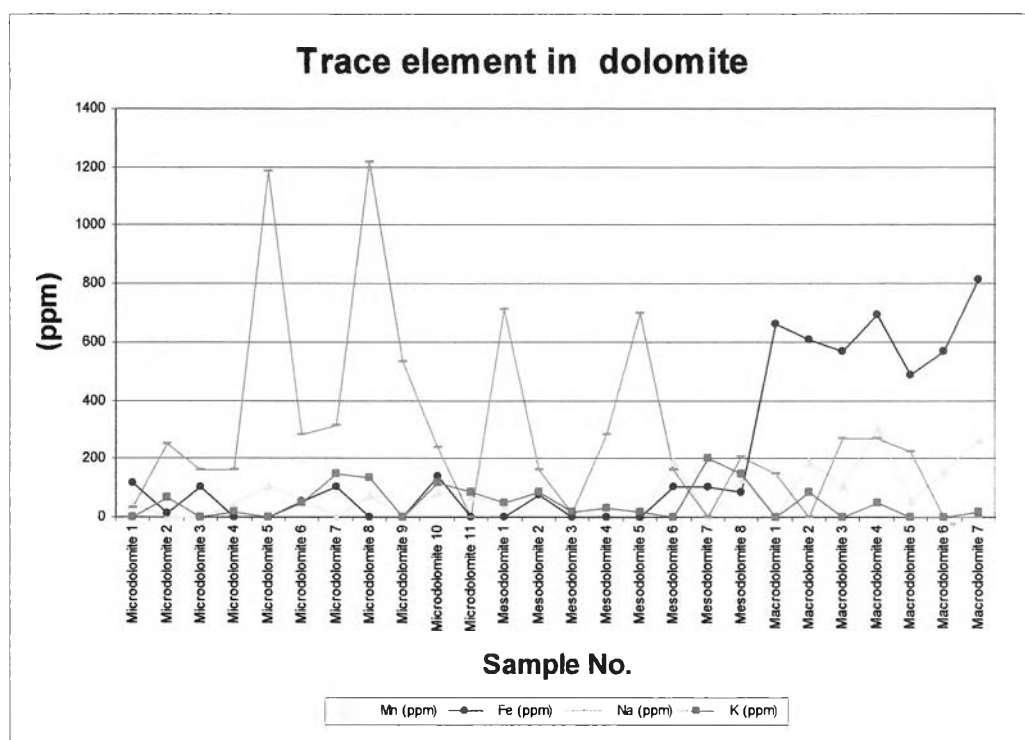
Figure 6.10 The trace element concentrations in microcrystalline, mesocrystalline and macrocrystalline dolomites.
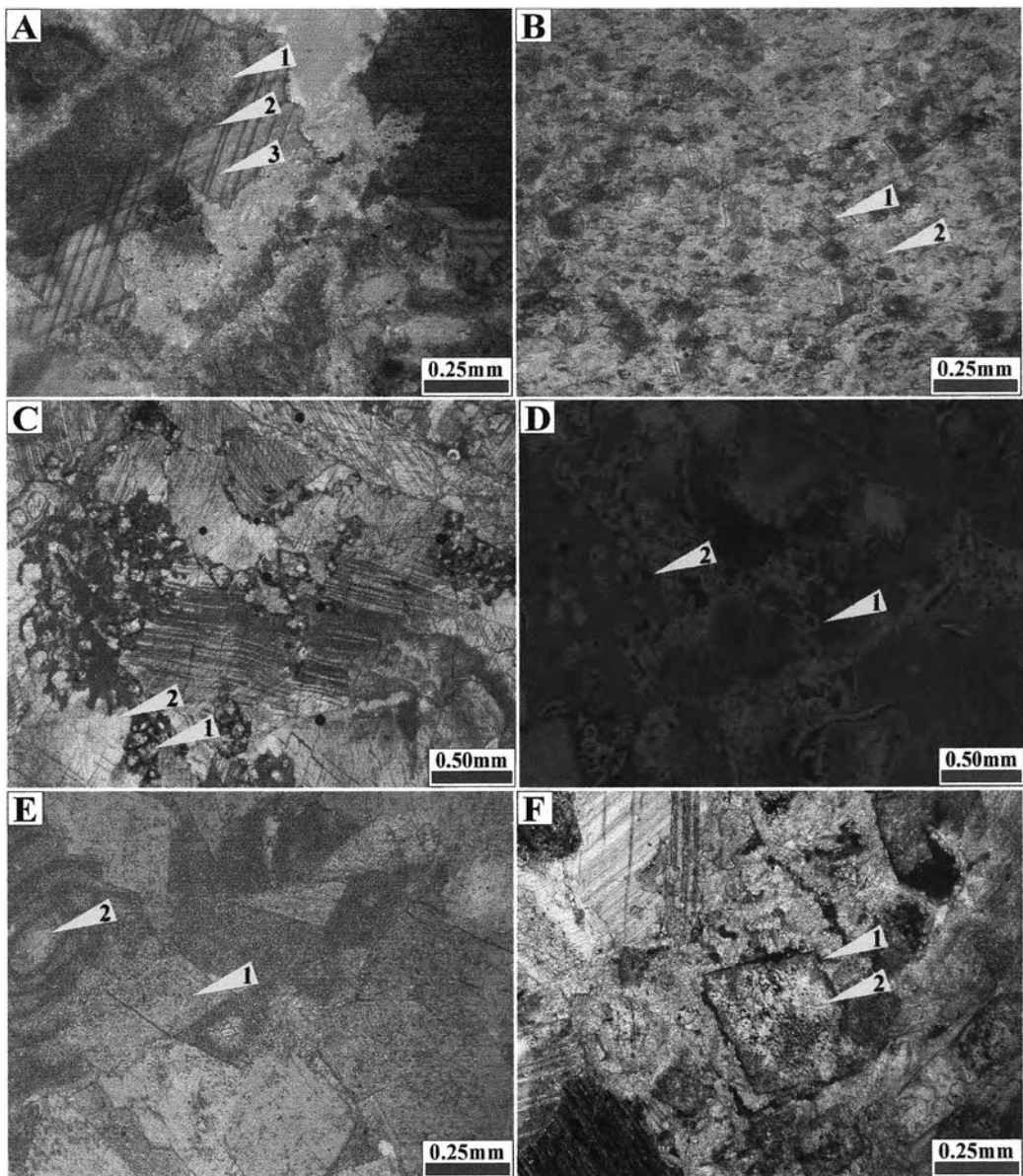
Figure 6.11 **A**: Photomicrograph of stained silicified crinoidal biosparite showing
abundant microcrystalline dolomite (A) formed along a dissolution surface (2)
of syntaxial overgrowth grain (3). (Stained, PPL); **B**: Photomicrograph of
silicified limestone showing mesocrystalline dolomite rhombs (1) embedded
in microcrystalline quartz (2). (PPL); **C**: Photomicrograph of dolomitic
crinoidal biosparite showing sparsely distributed mesocrystalline dolomite
rhombs (1) associate with syntaxial overgrowths calcite cement (2). (PPL); **D**:
Cathodoluminescence of C showing bright red luminescence zoning (1)
around mesocrystalline dolomite. Some of dolomite rhombs have core of non-
luminescence zone (2). (CL); **E**: Photomicrograph of stained dolomitic
biosparite showing macrocrystalline dolomite (1) replaced fusulinid grain (2)
and cement. (Stained, PPL); **F**: Photomicrograph of dolomitic biosparite
showing abundant impurity (1) around dolomite rhombs (2). (XPL)

The trace element compositions of microcrystalline dolomite (11 samples) are summarized in Table 6.13 and details are in Appendix A. They contain high concentrations of Na and low contents of Ba, Fe, Mn, K and Si. The Sr is lower than the detection limit of EPMA

Table 6.13 Summary of trace element composition of microcrystalline dolomite

	Elemental composition of microcrystalline dolomite (ppm)									
	Ca	Mg	Fe	Mn	Na	Sr	Ba	K	Si	Total
Min	219,482.31	66,421.59	0.00	0.00	0.00	0.00	0.00	0.00	0.00	339,859.98
Max	310,827.26	120,182.54	139.92	108.42	1,216.64	0.00	259.74	149.43	32.72	384,600.41
Average	250,447.37	109,571.05	48.05	45.06	397.90	0.00	73.28	55.85	8.92	360,647.49
SD	30,028.64	19,705.19	56.03	39.61	422.31	0.00	108.14	57.64	12.96	13,295.19

6.6.4.2 Mesocrystalline Dolomite

The mesocrystalline dolomite appears as euhedral to subhedral crystals of 10-200 μms in size. The majority of mesocrystalline dolomite occurs in close association with microcrystalline dolomite and some forms as rhombs partly disseminated in fine-grain chert matrix (Figure 6.11B). These dolomite crystals also isolated or clusters floating within the micrite matrix. They found in the unit KD1, KD2, KD4, KD5, KD6, KD7, KC2, KC3, KC4, KC5, KC7, PK1, PK2 and PK3.

The trace element compositions of mesocrystalline dolomite (8 samples) are summarized in Table 6.14 and details are in Appendix A. They contain high concentrations of Na, moderate contents of and low contents of K Mn, Fe, Si and Ba. The Sr content is below the detection limit of EPMA. The mesocrystalline dolomite luminaces bright red on the overgrowth zone with some non-luminaced cores (Figures 11C and 11D).

Table 6.14 Summary of trace element composition of mesocrystalline dolomite.

No.	Elemental composition of mesocrystalline dolomite (ppm)									
	Ca	Mg	Fe	Mn	Na	Sr	Ba	K	Si	Total
Min	228,065.78	121,563.81	0.00	0.00	0.00	0.00	0.00	0.00	0.00	352,568.24
Max	239,886.80	127,191.43	101.05	185.87	712.18	0.00	125.39	199.24	51.42	361,596.97
Average	231,010.31	124,086.59	45.67	58.08	280.05	0.00	15.67	68.49	28.05	355,592.91
SD	3,823.59	2,238.76	49.41	69.89	278.30	0.00	44.33	71.24	18.86	2,686.96

6.6.4.3 Macrocrystalline Dolomite

The macrocrystalline dolomite is the most abundance and occurs as partial or total replacement on former carbonate grains, matrix and cements (Figure 11E). The macrocrystalline dolomite has various sizes (commonly larger than 200 µms) and forms perfect crystal faces invading other grain components, except quartz. Some of them show gently curved crystal faces and cleavage planes with sweep extinction known as diagenetic baroque or saddle dolomite (Radke and Mathis, 1980). The crystals usually show cloudy core and clearer rim following the growth zones. They are found in the unit KD2, KD6, KC2, KC9 and PK2. It is noted that some dolomite rhombs show corroded rim with abundant impurity (Figure 11F).

The trace elemental compositions of macrocrystalline dolomite (7 samples) are summarized in Table 6.15 and details are in Appendix A. They contain high concentrations of Fe, moderate contents of Mn, Na and low Ba, Si and K content. The Sr content is below the detection limit of EPMA.

Table 6.15 Summary of trace element compositions of macrocrystalline dolomite.

No.	Elemental composition of macrocrystalline dolomite (ppm)									
	Ca	Mg	Fe	Mn	Na	Sr	Ba	K	Si	Total
Min	214,679.57	115,146.03	489.71	0.00	0.00	0.00	0.00	0.00	0.00	337,180.74
Max	245,011.16	122,034.29	816.18	302.04	267.07	0.00	277.66	83.01	65.45	365,293.06
Average	229,573.78	119,177.82	628.51	152.68	129.29	0.00	89.57	21.35	24.71	349,797.71
SD	9,302.43	2,223.34	106.05	108.49	127.26	0.00	105.60	32.81	22.70	8,737.03

The macrocrystalline dolomite luminaces brighter red than the crosscutting calcite vein in which the calcite crystals in that vein appears as dull multi-colored zones grown from the wall (Figures 6.12A and 6.12B). Syntaxial overgrowth and macrocrystalline dolomite also luminace bright red (Figures 6.12C and 6.12D). It appears that the dolomite rhombs luminaces brighter red than other fabrics. The original crinoid fragments usually luminace dull red. However, the mottled bright and dull red luminescences are also observed in the crinoid grains. Overgrowth cement commonly shows bright zoned luminescence.

Interpretation: The microcrystalline dolomite could be considered to be a relatively early diagenetic feature, as it filled in burrow and predated the mesocrystalline dolomite and sparry calcite cement. However, some burrows postdated the microcrystalline dolomite which also supports the early stage formation of this type of dolomite. Dolomite is commonly formed in shallow saline depositional environments, frequently in relation to intense evaporation (Behrens and Land, 1972; Friedman, 1980; and McKenzie, 1981). Khantaprab (1972) described a small amount of very fine-grained (5 μms) euhedral and subhedral dolomites found embedded in the microcrystalline cement and matrix of the Umm Shaif oil field, Abu Dhabi marine area, Persian Gulf. In modern marine environment, Mayers (1987) reported the cryptocrystalline magnesian calcite cemented beach rocks as marine vadose cement in Hawaii that had similar texture as the microcrystalline dolomite. The high magnesian
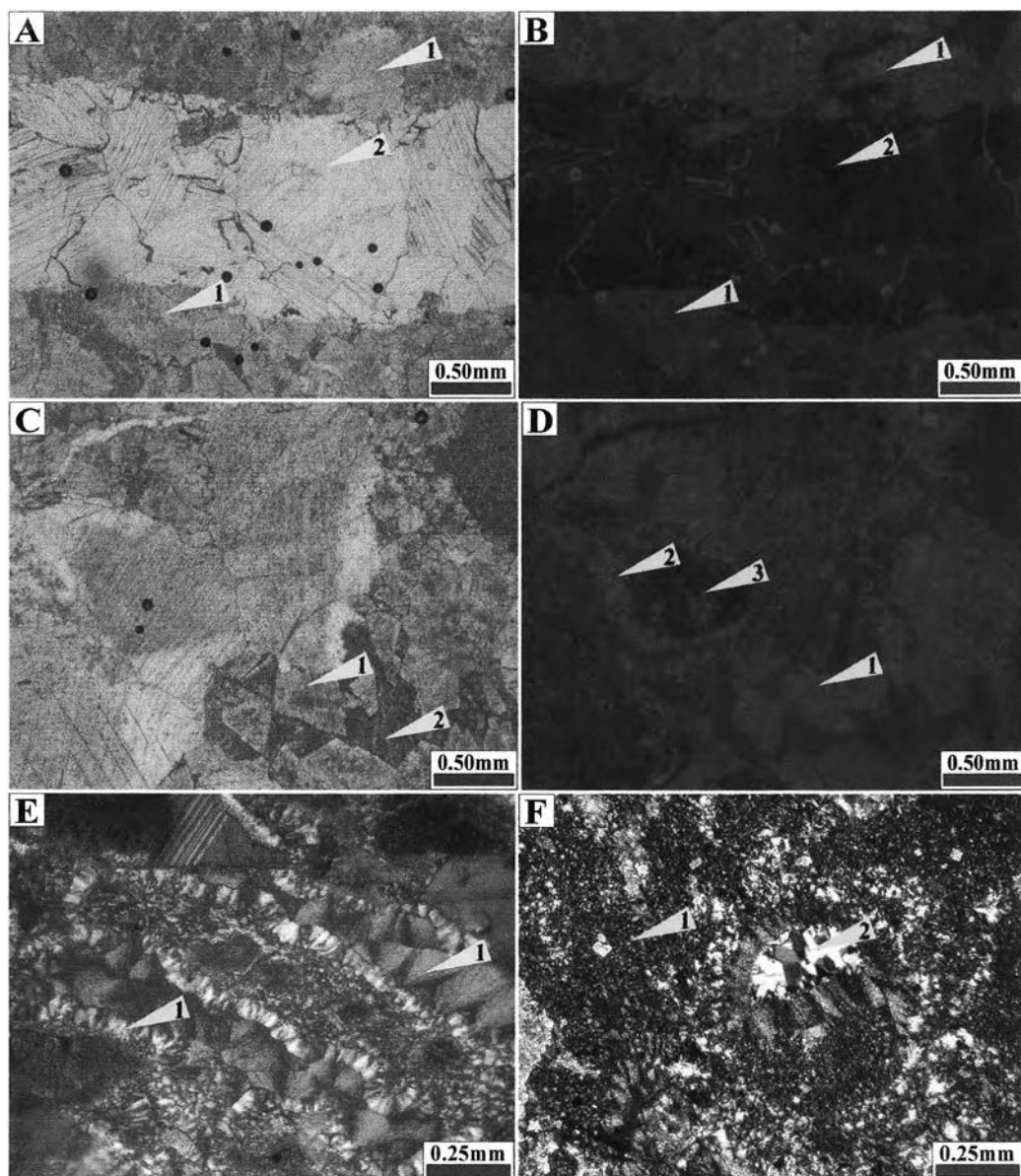
Figure 6.12 **A**: Photomicrograph of macrocrystalline dolomite (1) and a crosscutting calcite vein (2). (PPL); **B**: Cathodoluminescence of A showing bright red luminescence of dolomitized (1) zone as compared to dull red luminescence of calcite vein (2). The multiple parallel zoning reveals crystal growth structure from side wall of the vein. (CL); **C**: Photomicrograph of dolomitic poorly-washed crinoidal biosparite showing macrocrystalline dolomite (1) commonly replaced in micritic part (2). (PPL); **D**: Cathodoluminescence of C showing the different luminescent textures of macrocrystalline dolomite (1), the syntaxial overgrowth cement (2) and its original crinoid grain (3). The crinoid fragments show somewhat mottled luminescence. (CL); **E**: Photomicrograph of silicified limestone showing fibrous chalcedonic quartz (1) replaces the former carbonate components. (XPL); **F**: Photomicrograph of silicified limestone consisting of mostly microcrystalline quartz (1) and partly megacrystalline quartz (2). (XPL)

calcite was likely to transform into low magnesian calcite or dolomite due to the unstable form of high magnesian calcite in that condition. So, it was suggested that the microcrystalline dolomite could replace precursor cryptocrystalline or micrite cement in supratidal to intertidal setting during early diagenesis (Carballo et al., 1987; Mazzullo et al., 1987; Thériault and Hutcheon, 1987, and Smith and Simo, 1997). The source of Mg^{2+} for the microcrystalline dolomitization might have been from highly saturated marine brine which was largely available in a restricted marine environment (Machel and Mountjoy, 1986; Amthor and Friedman, 1991, 1992; Lawrence, 1994; Purser et al., 1994; and Reinhold, 1998). The highly saturated brine was necessary to create a number of nucleation points of microcrystalline dolomite (Sibley and Gregg, 1987).

The mesocrystalline dolomitization might have occurred during shallow burial diagenesis while the macrocrystalline dolomite could have formed during deep burial diagenesis by the replacement of pre-existing carbonate components (Zenger, 1983; Gregg and Sibley, 1984; Thériault and Hutcheon, 1987; Moore, 1989; and Amthor and Friedman, 1992). The precipitation of dolomite from modified seawater in the shallow burial, soon after deposition, has been discussed by Bone et al. (1992), James et al. (1993), Mazzullo et al. (1995) and Nicolaides (1997). The comparative coarse grain dolomite crystals represent a decrease saturation of brine with few nucleation points (Sibley and Gregg, 1987; and Baird, 1992). The source of Mg^{2+} could have been released from the transformation of metastable high-Mg calcite to low-Mg calcite during the burial diagenesis (Mišík, 1993; and Giménez-Montsant et al., 1999). The higher concentration of Fe in macrocrystalline dolomite as, compared to other dolomites was expected due to formation in anoxic condition of pore fluid with high Fe content. The Baroque or saddle dolomites have been considered to be burial phenomena (Török, 2000) which indicated diagenetic temperature between 60 – 150 °C (Radke and Mathis, 1980).

6.6.5 Silicification

One of the most important diagenetic features observed in this study is the partial silicification of carbonate rocks. There are three kinds of silicified fabrics distinguishable under a microscope, called chalcedony, microcrystalline and magacrystalline quartzes (Folk and Weaver, 1952; Hesse, 1989). They are found throughout the Khao Khad formation except in the unit KD2, KD4, KD7 and KC2.

6.6.5.1 Chalcedonic Quartz

The chalcedony or chalcedonic quartz is a radiating or sheaf-like bundle of fibrous silica of few μms up to 200 μms in length (Figure 6.12E). The sheaves locally include patches of cryptocrystalline and microcrystalline quartzes, which may be the manifestation of optical orientation of the chalcedonic fibers parallel to the microscope axis.

6.6.5.2 Microcrystalline Quartz

The microcrystalline quartz is an aggregate of very finely crystalline silica of less than ten μms in diameter and usually shows undulatory extinction. This type of quartz forms as the bulk of most chert nodules (Figure 6.12F).

6.6.5.3 Megacrystalline Quartz

The megacrystalline quartz is well-defined crystals of authegenic α-quartz showing absence crystallographic complexities as commonly found associate with the microcrystalline quartz or the fibrous silica. It is characterized by interlocking crystals of equant to elongate megaquartz ranging in size from 10 to 500 μms. The

megacrystalline quartz occurs as drusy quartz crystals or as intergrowth crystals filling in cavities of fossils (Figure 6.13A).

The trace element compositions of authegenic quartz (58 samples) are summarized in Table 6.16 and details are in Appendix A. They contain low concentrations of most trace elements except Ca.

Table 6.16 Summary of trace element compositions of authegenic quartz

| | Elemental composition authegenic quartzs (ppm) | | | | | | | | | |
	Ca	Mg	Fe	Mn	Na	Sr	Ba	K	Si	Total
Min	0.00	0.00	0.00	0.00	0.00	0.00	0.00	0.00	288,019.50	441,274.14
Max	152,815.72	355.87	233.19	147.15	341.25	0.00	268.70	547.90	472,070.00	473,549.27
Average	7,115.02	29.64	50.93	25.10	85.19	0.00	57.91	98.47	449,848.47	457,310.72
SD	22,939.37	58.68	59.61	40.91	102.48	0.00	78.37	87.52	25,542.20	5,036.45

Interpretation: The biogenic origin of chert has been widely accepted (Hein et al., 1978, 1981; Bustillo and Ruiz-Ortiz, 1987; Maliva et al., 1989; Mukhopadhyay et al., 1999) Dissolution of siliceous skeletons, local migration and precipitation of silica could involve in the silicification or chertification of carbonate rocks. The source of silica might have been the remains of siliceous skeletons in fossiliferous carbonate rocks, such as radiolarian tests, sponge spicules (Geeslin and Chafetz, 1972; Meyers, 1977; Bustillo and Ruiz-Ortiz, 1987; Maliva and Siever, 1989; Gao and Lan, 1991; and Lawrence, 1994) which were originally composed of metastable amorphous opal-A (Calvert, 1971). It is therefore important to note that abundant sponge spicules have been found in the unit KD1, KD9 and KC8 which are not intensely silicified (Figure 6.13B). The siliceous matters could be dissolved at pH values greater than 9 at or near seawater sediment interface (Kastner, 1981) during active photosynthesis of indigenous algae (Blatt et al., 1972). For example, the pH value as high as 10.2 was recorded in the Coorong Lagoon of South Australia (Peterson and Von Der Borch,
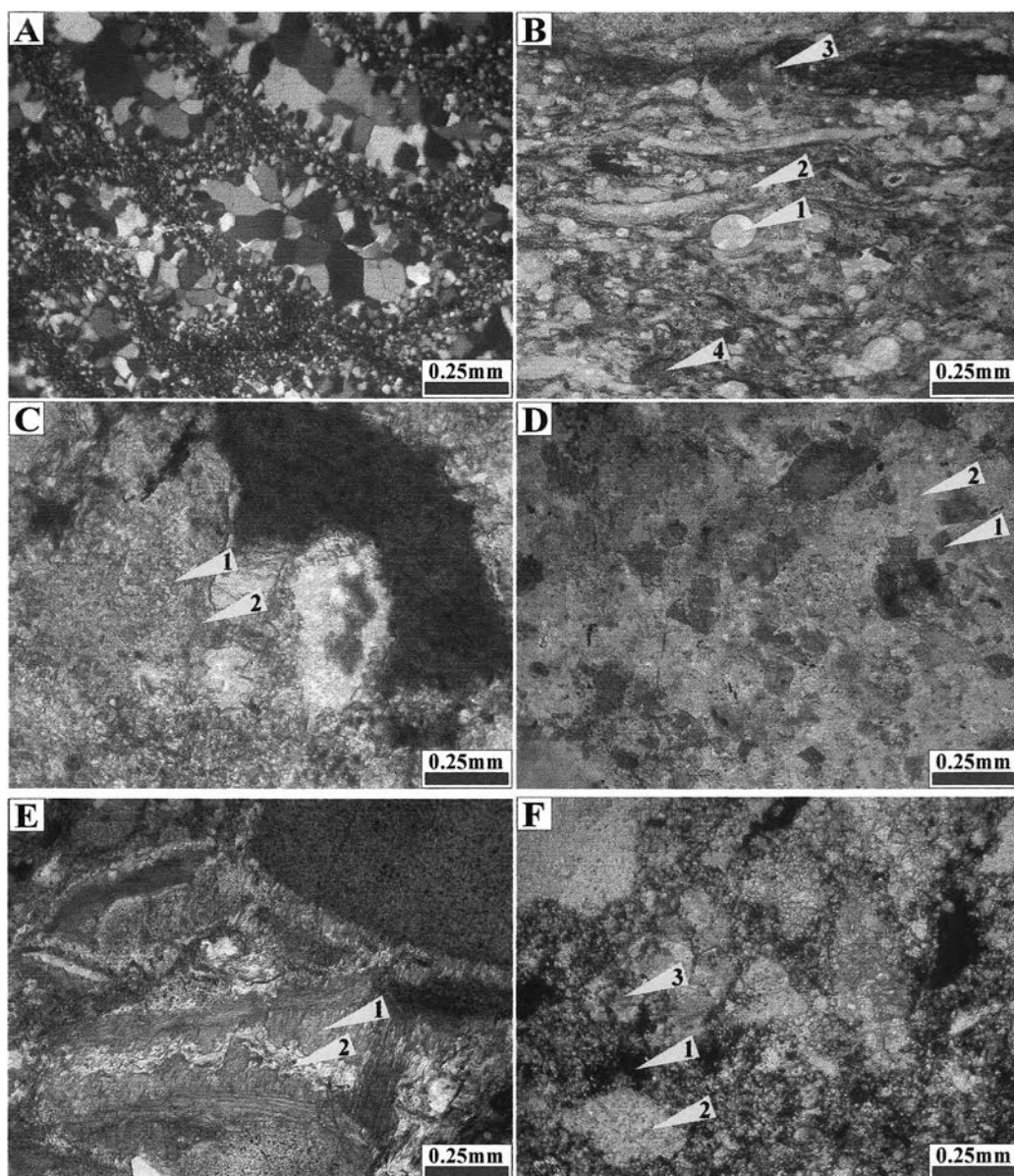
Figure 6.13 **A**: Photomicrograph showing the megacrystalline quartz completely replaces former carbonate components in a fusulinid shell. (XPL); **B**: Photomicrograph of stained silicified limestone composed of abundant siliceous sponge spicules (1) in fine grain sediments (2) with some calcareous fragments (3) and ferroan calcite (4). (PPL); **C**: Photomicrograph of stained dolomitic crinoidal biosparite containing abundant calcite rhombs (1) embedded in microcrystalline dolomite (2). (Stained, PPL); **D**: Photomicrograph showing abundant ferroan calcite rhombs (1) embedded in microcrystalline quartz (2). (Stained, PPL); **E**: Photomicrograph of stained crinoidal biosparite showing the dissolution feature on ferroan calcite cement (1). The dissolution pathway is filled by microcrystalline quartz (2). (Stained, PPL); **F**: Photomicrograph of stained micro breccia showing dull and dirty corroded surface packed with residual clay (1) known as vadose silt surrounding residual calcareous grains (2). The ferroan calcites (3) are commonly associated with vadose silts. (Stained, PPL)

1965). In this alkaline environment the siliceous sponge spicules and other siliceous skeletons were leached. However, below the seawater-sediment interface in the shallow burial condition the pH could reduce to as low as 6.5 following the decay of organic matter (Peterson and Von Der Borch, 1965; and Reinhold, 1998). The decrease in pH and/or decrease in volume of solvent (water) could cause the silica in solution to precipitate, thus forming an amorphous gel containing cristobalite crystallites or opal-CT (Blatt et al., (1972) before crystallizing as quartz chert (Mizutani, 1977). Therefore during the early diagenesis, the carbonate skeletals could be dissolved under the decreasing pH condition and replaced by the mobilized silica in the shallow burial condition. The silica phase changed from opal-A to opal-CT and from opal-CT to quartz (Maliva and Siever, 1988).

6.6.6 Calcitization

Calcitization or dedolomitization is the process of conversion or replacing dolomite by calcite. It is not widely observed in this study. The diagnostic feature indicating the dedolomitization process is the euhedral to subhedral rhombs of calcite (30-100 μms in size) within micrite or chert matrix (Figure 6.13C), similar to the fabric observed in mesocrystalline dolomite described earlier (Figure 6.13D). However, most of the embedded rhombs are still dolomite, only some parts have been replaced by both ferroan and non-ferroan calcite. The latter was found both in part of former dolomite rhombs and calcite cement (Figure 6.13E).

The trace element compositions of calcitized/dedolomite (29 samples) are summarized in Table 6.17 and details are in Appendix A. They contain high concentrations of Fe, Mn, Na and K, and low contents of Mg and Ba. The Sr content is below the detection limit of EPMA

Table 6.17 Summary of trace element compositions of calcitized/dedolomite rhombs

	Elemental composition of calcitized/dedolomite rhombs (ppm)									
	Ca	Mg	Fe	Mn	Na	Sr	Ba	K	Si	Total
Min	377,829.76	0.00	0.00	0.00	0.00	0.00	0.00	0.00	0.00	380,992.22
Max	418,381.46	1,900.00	2,689.51	1,773.51	1,632.07	0.00	232.87	398.47	28,300.36	421,009.16
Average	396,828.28	91.52	547.07	272.93	300.83	0.00	29.65	133.97	3,569.02	401,773.26
SD	11,196.89	374.91	757.37	359.61	431.95	0.00	61.55	116.13	8,158.24	11,974.60

Interpretation: The presence of calcite pseudomorph after dolomite in limestone, or dedolomitization, had been widely recognized (e.g. Evamy, 1963, 1967; Goldberg, 1967; Al-Hashimi and Hemingway, 1973; Frank, 1981; Back, et al., 1983; Budai et al., 1984; Thériault and Hutcheon, 1987; Kenny, 1992; Mišík, 1992; Colson and Cojan, 1996; Reinhold, 1998; and Arenas et al., 1999). It was a replacement process under the influence of meteoric water by which the rhombic dolomite precursor were partially dissolved and subsequently filled by sparry calcite during diagenesis at difference times from early to late diagenesis (Thériault and Hutcheon, 1987). The trace element analysis shows high concentration of Fe, moderate concentration of Na and Mn, and low concentration of Mg which suggests a meteoric water condition. The $\delta^{18}O$ values of late ferroan calcite cement associated with calcitized dolomite rhombs (-16.75 to -11.68 ‰PDB with an average -14.03 ‰PDB) also support the evidence of meteoric influence. The late calcite cements related to calcitization processes also mentioned by Thériault and Hutcheon (1987). The occurrence of mesocrystalline and macrocrystalline dolomite rhombs partially to completely replace by ferroan calcite has suggested that the calcitization process took place after macrocrystalline dolomitization and the process was likely to occur in meteoric phreatic zone during late diagenesis.

6.6.7 Dissolution

The dissolution process might have taken place several times throughout the diagenetic history. They are recognized as corroded rims of some diagenetic fabrics. The dissolution process could occur in two distinctive environments, i.e. under phreatic or vadose zones of meteoric water. Under the phreatic zone, the dissolution feature appears as clear and clean corroded surface surrounding syntaxial cement (Figures. 6.11A and 6.13C). The dissolution feature in vadose environment, which is the most distinctive, shows as dull and dirty corroded surface packed with residual clay known as vadose silt surrounding syntaxial cement (Figure 6.13F). These fabrics therefore indicate that the sediments were emerged above sea level and could be dissolved by meteoric water under both phreatic and vadose conditions.

6.6.8 Neomorphism

All the carbonate rocks in the study area have been affected by neomorphism to certain degree, especially in the area along Pak Chong – Khao Yai route. This process is recognized by the presence of recrystallized micrite grains (usually 3 to 6 μms and some up to 10 μms in size). For examples, most micritized walls of fusulinid tests were recrystallized into 10 μms in size which have obscured the original structure (Figure 6.14A). In the neighboring area along the Pak Chong – Khao Yai route, most of micrite and micritic shells were intensely coalescive neomorphosed in which the micrite as well as other diagenetic fabrics were recrystallized into microspars of various sizes (commonly 30 to 50 μms). It is noted that there are many stocks of intrusive rock in the neighboring Khao Yai area.

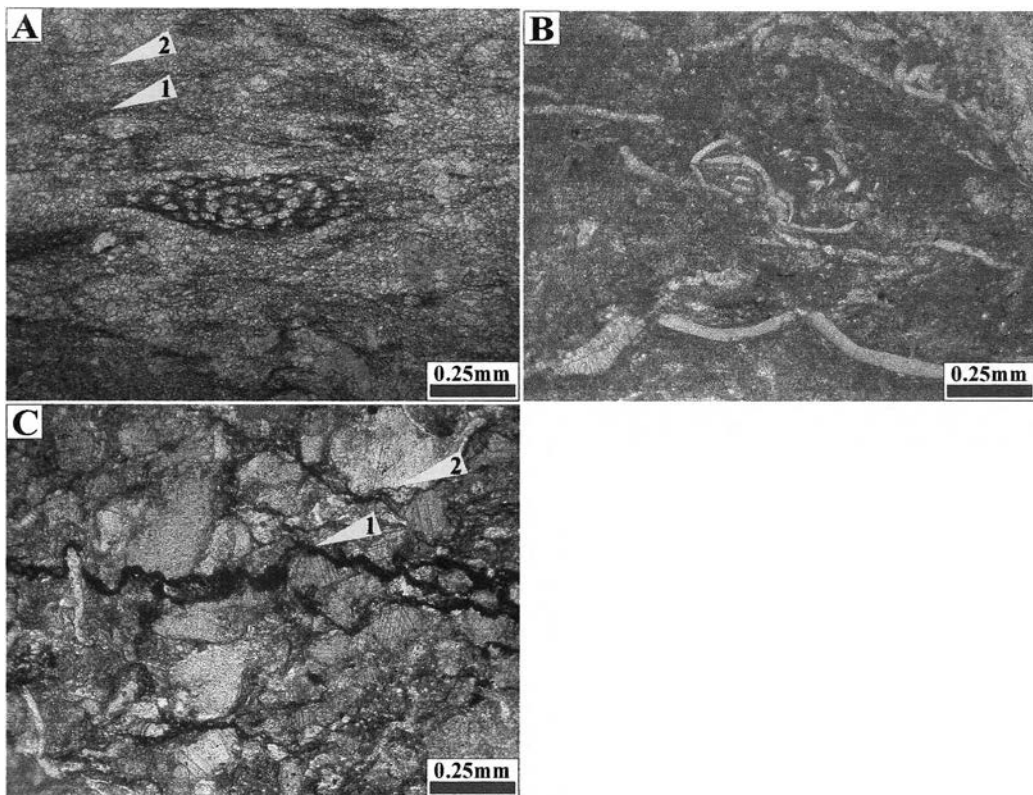Figure 6.14 **A**: Photomicrograph of neomorphic biomicrite showing aggrading neomorphism of former micrite matrix (1) and micritized grains (2). (PPL); **B**: Photomicrograph of stained biomicrite containing broken shell fragments due to burial compaction load. (PPL); **C**: Photomicrograph of stained intramicrite showing zigzags stylolite (1) and micro-stylolite features caused by compaction dissolution. (PPL)

The trace element compositions of neomorphic calcite in matrix (25 samples) are summarized in Table 6.18 and details are in Appendix A. They contain high concentrations of Si, moderate contents of Mn, Na and Fe, and low contents of Ba and K. The Mg and Sr contents are below the detection limits of EPMA.

Table 6.18 Summary of trace element compositions of neomorphic calcite in matrix

	Elemental composition of neomorphic calcite in matrix (ppm)									
	Ca	Mg	Fe	Mn	Na	Sr	Ba	K	Si	Total
Min	388,285.72	0.00	0.00	0.00	0.00	0.00	0.00	0.00	0.00	388,916.81
Max	414,986.66	0.00	349.79	797.69	474.79	0.00	322.44	332.06	11,013.49	415,586.98
Average	400,225.10	0.00	106.03	150.55	146.00	0.90	64.85	64.42	1,282.91	402,039.86
SD	8,214.19	0.00	112.28	183.35	161.72	0.00	88.30	99.88	3,017.04	9,115.17

The trace element compositions of neomorphic calcite in grains (13 samples) are summarized in Table 6.19 and details are in Appendix A. They contain moderate concentrations of Fe and Mn, and low contents of Si, K, Na and Ba. The Mg and Sr contents are below the detection limits of EPMA.

Table 6.19 Summary of trace element compositions of neomorphic calcite in grains

	Elemental composition of neomorphic calcite in grains (ppm)									
	Ca	Mg	Fe	Mn	Na	Sr	Ba	K	Si	Total
Min	401,922.07	0.00	0.00	0.00	0.00	0.00	0.00	0.00	0.00	402,268.66
Max	419,439.20	0.00	707.36	325.27	267.07	0.00	107.48	298.85	271.13	419,764.54
Average	412,100.95	0.00	175.19	128.08	50.22	0.00	15.85	58.75	62.93	412,591.97
SD	5,758.48	0.00	202.96	99.21	89.13	0.00	33.94	90.33	77.68	5,775.95

6.6.9 Compaction

The compaction features found in the rock of the Khao Khad Formation can be categorized into two types, namely, mechanical compaction and chemical compaction. The mechanical compaction is not particularly common, but can be found in biomicrite and biomicrudite. It is recognized as grain breakage or collapse of shell such as fusulinid tests and brachiopod shells. They are found in the units KD3, KD6, KC1 and PK1. It postdated micritization and micrite envelope. For example, the micritized brachiopod shells were broken in micrite matrix (Figure 6.14B) and some micrite-coated fusulinid tests were broken in micrite matrix. The broken shells were finally cemented by coarse sparry calcite cement (Figure 6.5F).

The chemical compaction features are more common than the mechanical compaction features. They are found as stylolites in the units KD5, KC7, KC8, KC9, PK2 and PK3. The stylolites can be recognized occasionally in dolomitic limestone in which the mesocrystalline dolomite rhombs lining along the stylolitic surface and forming zigzag suture line (Figure 6.14C). It can also be found in packed biomicrite, biosparite and intrasparite. The stylolites are difficult to identify in the field due to the nature of outcrop of limestone that are often weathered out. However, it is easy to see on the fresh surfaces.

Interpretation: The mechanical compaction was not common in the Khao Khad Formation. This may be due to the cementation produced during early diagenesis made an early rigid framework of sediments. The fabrics related to compaction, such as grain breakage and collapse of shell, are probably the product of slightly compactional force during early burial diagenesis prior to lithification of micrite matrix. The presence of micrite protrudes into the internal chamber of fusulinid tests as internal sediment or as geopetal structure indicates that they were deposited in

unconsolidated micrite matrix. The broken grains were compacted after grains were buried in incompletely indurate micrite matrix. Then the chambers of the host grains were broken and micrite matrix with broken shell fragments invaded into the chambers. The presence of mesocrystalline dolomite accumulated and bound along stylolites line indicated that the stylolites postdated the mesocrystalline dolomitization. The compaction caused the dissolution of calcareous parts and left the dolomite rhombs as residual along the dissolution surface. This is a typical feature formed during burial diagenesis (e.g. Gregg and Sibley, 1984; Moore, 1989). The process of pressure-solution related to dolomitization often formed during burial diagenesis (e.g. Mattes and Mountjoy, 1980; Qing and Mountjoy, 1989; Lavoie and Bourque, 1993; Mountjoy and Amthor, 1994). It is therefore concluded that the compaction process mainly occurred during early burial diagenesis and late burial diagenesis.

6.7 Diagenetic Evolution

The diagenetic history of the Khao Khad Formation has been complicated by repeated diagenetic cycles involving both dissolution and precipitation. Most of the diagenetic processes probably occurred before deep burial and predominantly influenced by marine water condition. In general the development of the later diagenetic fabrics causes partial obliteration of the earlier diagenetic fabrics. Hence the diagenetic sequence of rocks in the study area can apparently be subdivided into two phases, early diagenesis and late diagenesis and is displayed graphically in Figure 6.15. The early diagenesis or syndepositional diagenesis is here defined as the changes occurred immediately after sedimentation with the influence of sedimentary environment continuing to early stage of compaction and cementation in shallow burial condition. The late diagenesis or deep burial digenesis is referred to the changes occurring at deep burial and above the realm of low-grade metamorphism.

Diagenetic processes	Relative time		
	Early		Late
1) Grain abrasion	▰ ▰		
2) Micritization	▰		
3) Microcrystalline calcite cement	▰ ▰		
4) Meniscus cement	▰		
5) Acicular fibrous cementation	▰		
6) Burrowing	▰		
7) Microcrystalline dolomite	▰		
8) Radiaxial ficrous calcite cement	▰		
9) Dog-tooth calcite cement	▰		
10) Early compaction	▰▰		
11) Equant calcite cement	▰		
12) Blocky calcite cement	▰		
13) Syntaxial overgrowth calcite cement	▰▰		
14) Grain dissolution	▰		
15) Microcrystalline dolomitization	▰		
16) Mesocrystalline dolomitization	▰		
17) Silicification	▰		
18) Macrocrystalline dolomitization		▰▰	
19) Calcitization/dedolomitization			▰
20) Ferroan calcitization			▰
21) Dissolution compaction		▰▰▰	

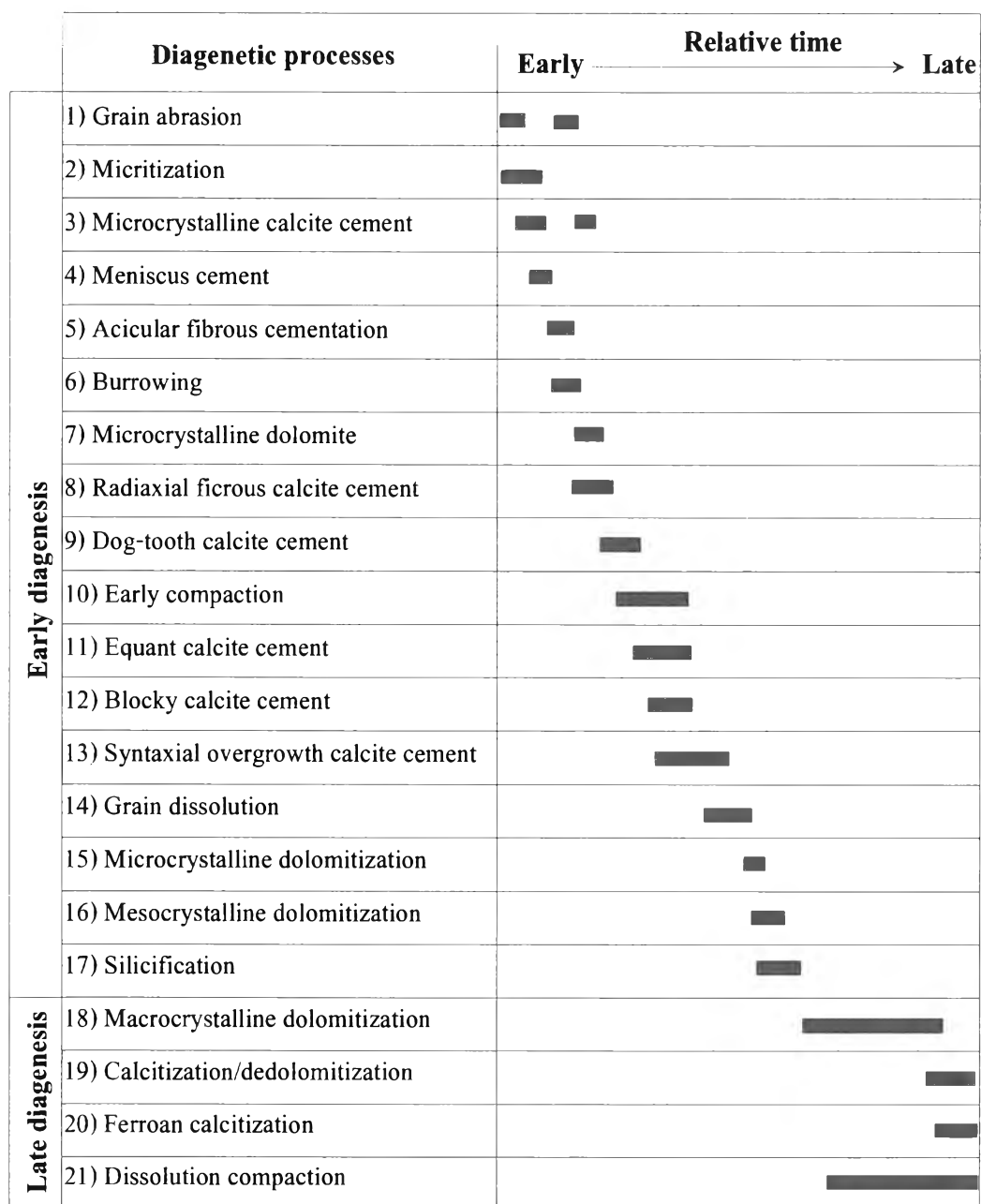Rows 1–17 labeled **Early diagenesis**; rows 18–21 labeled **Late diagenesis**.

Figure 6.15 Generalized diagenetic sequence of the Khao Khad Formation in relative time.

The neomorphism of pre-existing carbonate components took place throughout the diagenetic sequence.

6.7.1 Early Diagenesis

As the grains were deposited in shallow marine environments, they were subjected to some early diagenetic processes, such as grain abrasion, grain micritization, microcrystalline calcite cement, meniscus cement, acicular fibrous cementation, burrowing, microcrystalline dolomitization, radiaxial fibrous calcite cement, dog-tooth calcite cement, early compaction, equant calcite cement, blocky calcite cement, syntaxial overgrowth cementation, dissolution, microcrystalline dolomitization, mesocrystalline dolomitization, and silicification.

The early diagenetic processed can be described as follows:

1) Grain abrasion; it occurred in high-energy environment of intertidal zone and barrier bar by which some skeleton fragments such as fusulinid tests and crinoids, as the result of abrasion, might have an incomplete form and rounded-off rim.

2) Micritization; shortly after the deposition of allochems in the intertidal to subtidal of shallow marine environment, most of the grains were micritized and formed micrite-coated rims or micrite envelopes. However, some grains were completely micritized.

3) Microcrystalline calcite cement; in part of intertidal zone, the evaporation of seawater during low tide caused precipitation of microcrystalline high magnesian calcite cement which might transformed into microcrystalline calcite or microcrystalline dolomite later. The microcrystalline high magnesian calcite was

suggested to be the first marine vadose cement that cemented the intertidal sediments such as broken shells, pellets and algal stromatolites.

4) Meniscus cement; parts of sediments deposited in the intertidal zone were cemented by meniscus cement showing concave-like surfaces.

5) Acicular fibrous calcite cement; the first generation of submarine cementation could occur as acicular fibrous cement of formerly aragonite fringing around both intergranular and intragranular pores. They fringed around allochems and occluded the intragranular pores of fusulinid tests.

6) Burrowing; the burrows were found in semi-consolidated micrite deposits in zone of intertidal and subtidal environment.

7) Microcrystalline dolomitization; it was found associated with algal encrusted stromatolite and as geopetal filling in burrows. The microcrystalline dolomite was probably former high magnesian micrite or microcrystalline calcite. This calcite precipitated on the outer surface of algal stromatolite and filling as geopetal structure in burrows. During early diagenesis it was dolomitized into microcrystalline dolomite in the intertidal to supra tidal zone.

8) Radiaxial fibrous calcite cement; the radiaxial fibrous calcite cement was found on both intergranular and intragranular pore spaces, such as intergranular pore of the algal stromatolite and intragranular pore of fusulinid test. It replaced the former acicular high magnesian calcite in shallow marine environment.

9) Dog-tooth calcite cement; the dog-tooth calcite cement was found fringing around the surface of pore spaces during shallow burial.

10) Early compaction; as the sediments were accumulated through time in shallow burial condition, slight compaction caused collapse structures or broken grain components in the zone of poor cementation. The micrite matrix usually protruded into the internal pore space of broken shells due to semi-consolidated nature of the matrix.

11) Equant calcite cement; the equant calcite cement was found only as intragranular pore filling over the pre-existing cement. It was precipitated from a rather restricted pore fluid of presumably burial condition.

12) Blocky calcite cement; as the cementation continued the rest of both inter and intra granular pores were occluded by blocky calcite cement during burial marine phreatic condition.

13) Syntaxial overgrowth calcite cement; the cementation of most crinoid fragments took placed in the form of syntaxial rim overgrowth from the pre-existing grain surfaces in shallow burial marine environment. Some grains showed two generations of overgrowth cementation and following by grain abrasion under high-energy zone of barrier bar.

14) Grain dissolution; the sediments were then emerged above the sea level and the grains were partially dissolved by the meteoric water as seen from the dissolution rim of some crinoid fragments with some residual vadose silt.

15) Microcrystalline dolomitization; subsequently the formation of high magnesian calcite cement took place in the form of minute or meniscus cements around the grain surfaces and at the contact points of grains in marine vadose zone. Then the micrite cement might have been exposed to brine and was replaced by

microcrystalline dolomite on the dissolved surfaces in the intertidal to supratidal zones of shallow restricted marine environment.

16) Mesocrystalline dolomitization; subsequently, sediments were submerged to the shallow burial in marine phreatic environment. As the sediments submerged again, the transformation of some high Mg-calcite to low Mg-calcite might produce high Mg pore water which promoted the formation of mesocrystalline dolomite by replacing the pre-existing carbonate components.

17) Silicification; after the formation of mesocrystalline dolomite in shallow burial environment the dissolved silica originated from siliceous skeletals could replace the carbonates in the form of fibrous, microcrystalline and megacrystalline quartz cherts. As the sediments were subjected to shallow burial, slight compaction caused collapse structures or broken grain components in the zone of poor cementation.

6.7.2 Late Diagenesis

The processes occurred during late diagenesis are macrocrystalline dolomitization, calcitization or dedolomitization, ferroan calcitization, dissolution compaction, and neomorphism.

The detailed of late diagenetic processed can be described as follows:

18) After sediments were buried somewhat deeper, they might be in the marine phreatic zone under the influence brine water. Subsequently the macrocrystalline dolomitization probably took place during deeply burial environment by replacing pre-existing grains, matrix and cements.

19) Calcitization or dedolomitization; the macrocrystalline dolomitization was then post-dated by late calcitization as evidenced by some pre-curser dolomite rhombs being replaced by calcite, especially in the banded or nodular cherts during the late diagenesis.

20) Ferroan calcitization; the late stage calcite veins which were iron rich replaced both former calcite and dolomite and formed ferroan calcite and ferroan dolomite around the ferroan calcite vein. However, some ferroan calcite associated with stylolite.

21) Dissolution compaction; the late stage dissolution associated with burial compaction produced stylolite formation.